Bubble Rise in a Non-Isothermal Self-Rewetting Fluid and the Role of Thermocapillarity

Bubble Rise in a Non-Isothermal Self-Rewetting Fluid and the Role of Thermocapillarity

Dimitrios Mamalis[a,*], Vasileios Koutsos[a], Khellil Sefiane[a,b]

[a] Institute for Materials and Processes, School of Engineering, The University of Edinburgh, King's Buildings, Edinburgh EH9 3FB, United Kingdom

[b] Tianjin Key Lab of Refrigeration Technology, Tianjin University of Commerce, Tianjin City 300134, People's Republic of China

* To whom correspondence should be addressed: E-mail d.mamalis@ed.ac.uk

Abstract

We report on the motion of a buoyancy-driven bubble in a vertical micro-channel and the significant role of thermocapillarity. A series of experiments have been carried out using a circular micro-channel filled with pure liquids (pure water and pure 1-butanol) and a self-rewetting fluid (water – 1-butanol 5% vol.) under isothermal and non-isothermal controlled conditions. In both cases, different mass fluxes and heat fluxes were applied on the micro-channel within the same temperature gradient field (18 ºC to 75 ºC) which was increasing linearly in the same direction with the liquid flow. We have shown that the behaviour of the bubbles in a self-rewetting fluid departed considerably from that of pure liquids. The anomalous property of the alcohol mixture, i.e. the quasi-parabolic dependence of the surface tension with the temperature, drastically modified the movement (promoted or inhibited) and the shape (spherical or deformed) of the migrating bubbles. These phenomena were explained in terms of the location of the bubble associated with the well-defined surface tension

minimum, and as a function of dimensionless numbers. Heat transfer coefficient calculations in the single and two-phase flows were acquired for all the liquids used. We demonstrated that the presence of Marangoni stresses resulted in the enhancement of the heat transfer distribution in the self-rewetting fluid flows compared to the pure liquids.

1. Introduction

Bubbles and drops are relevant for a variety of engineering and materials process applications. In some cases, it is desirable to have a collection of bubbles within a material e.g. in polymer foams but in other situations, the aim is to produce a material free from inclusions such as a growing crystal. When gravity is present and the density of a dispersed liquid phase differs from that of a continuous phase, the dispersed phase material will shrink or expand if it is denser or less dense than the continuous phase e.g. bubbles in a fluid flow. Many experimental studies have been performed in space conditions where gravitational forces acting on bubbles or drops in a fluid phase are so small that can be neglected. There are a few mechanisms free of gravity that will cause a bubble or a drop in a liquid to move. For instance, an electric or magnetic field can be used to induce a motion to an object. The most common mechanism that has been used in many experimental works is the application of a temperature gradient field in a continuous phase. A temperature variation in a liquid phase can be achieved by heating or cooling the system.

The paramount importance of bubble flows is evident in chemical, biochemical, petrochemical and metallurgical industries applications such as bubble column reactors, drug delivery or cardiovascular systems [1–4]. Particular interest has been paid to the behaviour and the control of the motion of bubbles and drops in microfluidics, with a wide range of potential applications ranging from chemical analysis processes [5] to data processing [4]. The first study that was focussed on thermocapillary movement of migrating bubbles within a bulk liquid by

a temperature gradient, can be found in the pioneering work of Young *et al*. [6]. They performed experiments on air bubbles in a column filled with viscous fluid, silicone oil, heated from below and it was revealed that under the effect of thermocapillary force, small bubbles were seen to move downwards, whereas larger bubbles migrated in the opposite direction as buoyancy overcomes the thermocapillary effect [6]. They also provided a theoretical description of the bubble motion under the combined influence of gravity and thermocapillarity, in a downward temperature gradient, leading the bubbles to almost come to a standstill position [6]. Following the work of Young *et al*., numerous theoretical and experimental studies have been devoted to further understanding these interesting and complex phenomena [7–12]. The main motivation of the aforementioned studies is the formation of surface tension gradients due to temperature variations of a liquid-gas interface which induce tangential stresses, known as Marangoni flow, and drives flows in the vicinity of the interface [13–18]. The thermocapillary migration of bubbles and drops due to the generation of interfacial flows in a non-isothermal system can be of a significant importance in a great variety of technological applications.

It is well known that for ordinary fluids such as water, air and various oils, surface tension decreases almost linearly with increasing temperature. In contrast, for binary and generally multicomponent liquids, the physical behaviour poses many challenges, as it can be more complicated. Previous studies with liquids formed from binary mixtures of water with alcohols (methanol [19], ethanol [20–23] and 1-propanol [24]) showed a different behaviour compared to pure liquids. Vochten and Petre reported that for dilute aqueous solutions of high carbon alcohols (number of carbon atoms ≥ 4), the temperature dependence of the surface tension showed a minimum at certain temperatures (quasi-parabolic profile) [25]. This behaviour leads to a non-linear thermocapillary effect which was studied by Oron *et al.* [26] and later by Slavtchev and Miladinova [27]. Dilute aqueous solutions of alcohols such as

butanol, pentanol, hexanol etc. can be considered ‘‘self-rewetting” fluids because of the anomalous dependency of the surface tension on temperature with a well-defined minimum, in a range of concentrations [28,29]. Due to the presence of thermocapillary stresses (Marangoni effect) and the characteristic curvature of the surface tension-temperature, these alcohol mixtures ‘‘self-rewet” by moving rapidly towards the hot spots thus improve the wettability of the solid surfaces and consequentially enhance the rate of heat transfer. These binary alcohol fluids have recently been investigated and proposed as new operating fluids for advanced heat transfer applications, e.g. column reactors, heat pipes or heat spreaders for terrestrial and space devices [30–36]. In such non-azeotropic solutions for dilute concentrations, the alcohol-rich component preferentially evaporates in the course of liquid/vapour phase change, which results in a concentration gradient in the liquid/vapour interface. Liquid–vapour interface imbalances (concentration and/or temperature) lead to surface flows directed from the colder region to the hotter side, for temperatures beyond the minimum of the surface tension. In this case, the convection heat mechanism is driven by the reverse Marangoni effect. Thus, Marangoni effects may play an important role in energy heat transport phenomena [13–15,36–39].

Flows of multiphase systems provide several mechanisms for enhancing and extending the performance of single-phase ones. Such flows form when two or more partially or not miscible fluids are brought in contact and are subjected to pressure and/or temperature gradients. Multiphase flows occur in many operations in chemical, petroleum and power generation industries. Furthermore, the rapid development of microfluidic industry requires more effective cooling or heating methods to control the heat transfer mechanisms. However, the presence of gas bubbles in microfluidic systems can create major problems by disturbing and eventually blocking the fluid flows. The boundary interactions between the gas-liquid-solid phases introduce non-linearity and instabilities between the involved components. Previous studies have shown that different heat transfer profiles were reported depending on

various experimental conditions such as gravitational forces [6,32,34], channel geometry [40–42], working liquid [36,38,39], applied heat flux [43,44] or mass flux [40,43], etc. Understanding how bubbles affect the flow resistance in micro-channels is a way of determining the pumping or energy requirement for microfluidic devices where two-phase flow is involved, and therefore it is of fundamental and practical significance.

In this study, we investigate the motion of air bubbles travelling vertically in a temperature gradient field within a liquid continuous phase. We monitored the migration of induced air bubbles from the cold region (bottom of the channel) to the hotter region (upper side) along a circular glass micro-channel filled with different working fluids i.e. pure water, pure 1-butanol and water – 1-butanol 5% vol., and different mass fluxes in the same temperature gradient field. Furthermore, particular attention was paid to the thermocapillary migration of a deformable bubble within the micro-channel filled with a self-rewetting fluid that exhibits a non-linear (quasi-parabolic) dependence of the surface tension with the temperature. Our results indicate that in self-rewetting fluid flows, the bubble motion departs considerably from the pure liquids behaviour and the dynamics of the system becomes more complex. An experimental investigation on the local heat transfer coefficients, along the circular micro-channels was carried out, based on the high-speed visualization and infrared IR thermography. The results demonstrate that Marangoni stresses drastically influence the heat transfer profiles considering the buoyancy, inertia and viscous forces acting in the system.

Nomenclature

A	channel internal surface area	***Subscripts***	
A_c	cross sectional area	avg	average
C_p	specific heat capacity	$conv$	convective
d_c	channel diameter	eff	effective
d_{in}	channel internal diameter	env	environmental
d_{wall}	channel wall thickness	in	inlet, internal
h	heat transfer coefficient	W	wall
I	current	l	liquid
k	thermal conductivity	out	outlet
L_c	channel length	rad	radiative
ṁ	mass flow rate	x	distance to channel inlet
ϕ	mass flux	$S.P.$	single phase
Q	heat	$T.P.$	two phase
q	heat flux		
T	temperature	***Greek symbols***	
T_W	channel wall temperature	ε	emissivity
U	voltage	ρ	density
υ	velocity	ω	Stefan-Boltzmann constant
$\bar{\upsilon}$	average velocity	γ	surface tension
r_B	bubble radius	μ	dynamic viscosity
D_B	bubble diameter (width)	a	thermal diffusivity
L	channel's characteristic length	λ_c	capillary length

2. Experiments

2.1. Experimental apparatus and procedure

The first step in our experiments was to prepare aqueous solutions of pure alcohol: 1-butanol (Sigma-Aldrich 360465) with specific concentration: water – 1-butanol 5% vol. A circular channel with 145 mm length and 4 mm inner diameter was used, through which the requisite liquid was pumped in. The micro-channel was built from borosilicate glass and purchased by

VitroCom® Inc. The fluid delivery system was combined with a syringe pump to transfer the liquid through the flow loop at a controlled constant flow rate. The syringe pump device was provided by Cole-Palmer® Instrument Co, Ltd and the 100 mL borosilicate glass syringe was purchased from FORTUNA® Optima. The syringe was connected with the micro-channel by a plastic tube which was able to resist corrosion from the alcohol (butanol) phase and to operate at high temperatures up to 100 ^{o}C. Liquid was injected through the microchannel where it was subjected in a controlled temperature gradient field (from ~18 to 75±1 ^{o}C) and collected at the exit of the microchannel in a glass tank. A transparent, conductive, metallic deposit of tantalum, Ta, was sputtered on the exterior of the micro-channel hence enabling simultaneous uniform heating and visualisation of the flow inside the micro-channel. The Ta coating was micro-engineered in the Scottish Microelectronic Centre (SMC) with the use of an Oxford Plasmalab System® 400 magnetron sputtering system. More specifically, the thickness of the tantalum layer was optimized to ensure sufficient transparency for visualization while providing enough thermal energy for heating the micro-channel as desired. The film thickness was approximately 50 Å with an electric resistance ranging from 3 kΩ to 10 kΩ providing a power range of 1 – 10 W to the channel; using a high voltage (up to 300 V) and relatively low current ($I \leq$ ~0.05 A). The tantalum deposit was uniform both across and along the micro-channel and its thickness (a few nanometres) was negligible in comparison to the glass thickness of 1 mm. This allowed approximations to be made for the heat losses to the environment. The channel was connected by its ends to a DC power supply, enabling heating of the channel by passing a controlled current through the resistive tantalum coating, thus controlling the wall temperature along the channel. A programmable syringe was placed at the cold side (inlet) with a needle of 0.1 mm diameter in order to induce small controlled air bubbles in the fluid flow, as presented in Fig. 1 (a).

National Instruments® systems were adopted for data acquisition, connected to a computer and a LabVIEW® user interface. Inlet and outlet temperatures and pressures were monitored using K-type thermocouples and a pair of Omega® PXM219 series pressure transducers, respectively. Temperature and pressure data were acquired via a NI SCXI 1303 32-channel isothermal terminal block with a 166 kS/s maximum sampling rate and a NI USB-6009 Multifunction DAQ (up to 48 kS/s), respectively, connected to a data acquisition board on a PC. A CCD high-speed camera was set-up to visualise the flow formations. The high-speed camera employed was a NanoSense® MK III (IDT), with interchangeable macro and micro lenses, used as appropriate. The resolution of the camera allowed for either the entire heated micro-channel length to be captured or just a particular section of interest to be focussed upon. The rate of the camera was set from 500 fps to 2500 fps depending on different visualization requirements. The records extracted from the high-speed camera were analysed with the X-Vision (acquisition and image processing) software from IDT (Integrated Design Tools, Inc.). A cold light source (Fiber-Lite® illuminator) and Fiber Optic back light were put in conjunction with the high-speed camera providing a steady and uniform light intensity without releasing heat to interfere the thermal field around the micro-channel. A ThermaCam^{TM} infrared thermography system (SC3000 Series, FLIR® Systems, Inc.) was used to visualise and record the temperature profile at the micro-channel exterior wall. The IR camera offered ultra-high thermal sensitivity, broad dynamic range and long wave imaging. It is characterised by a measurement in the 8 – 9 μm band of the infrared spectrum with a high resolution of 320 x 240 pixels, thermal sensitivity of 20 mK at 30 ^{o}C, an accuracy of ±1 ^{o}C or 1% for temperature up to 150 ^{o}C, and is Stirling cooled. The camera operates at 50 Hz, therefore 50 frames per second were recorded. The infrared system provides automatic transmission correction of temperature, based on fixed parameters; atmospheric temperature, relative humidity, input distance from the object and emissivity of the object. The IR camera was used with an

appropriate lens and a dedicated PC for acquisition, with specialised software (ThermaCAM Researcher Professional®) for image processing. All the circular micro-channels used, were fabricated from borosilicate glass, which is an opaque material to IR radiation. An FTÅ200 Dynamic Contact Angle Analyzer (First Ten Ångstroms, Inc.) goniometer was also employed to measure the surface tension of the pure liquids as well as the 5% vol. butanol/water mixture by applying the pendant drop method analysis. This method involves the determination of the profile of a drop of one liquid suspended in another liquid or gaseous phase at equilibrium. The balance between gravity and the surface forces determines the profile of these drops. A minimum in surface tension as a function of temperature was measured at *ca*. 63 ºC for the water-butanol 5% vol. mixture. Fig. 1 (b) and (c) shows the results obtained for the surface tension-temperature dependence for all the liquids used in this experimental work. Both pure liquids and binary alcohol mixture were kept at a controlled temperature of 18 ±1 ºC, atmospheric pressure and relative humidity of RH = 40 ±10%. Fig. 1 depicts a schematic drawing of the experimental apparatus.

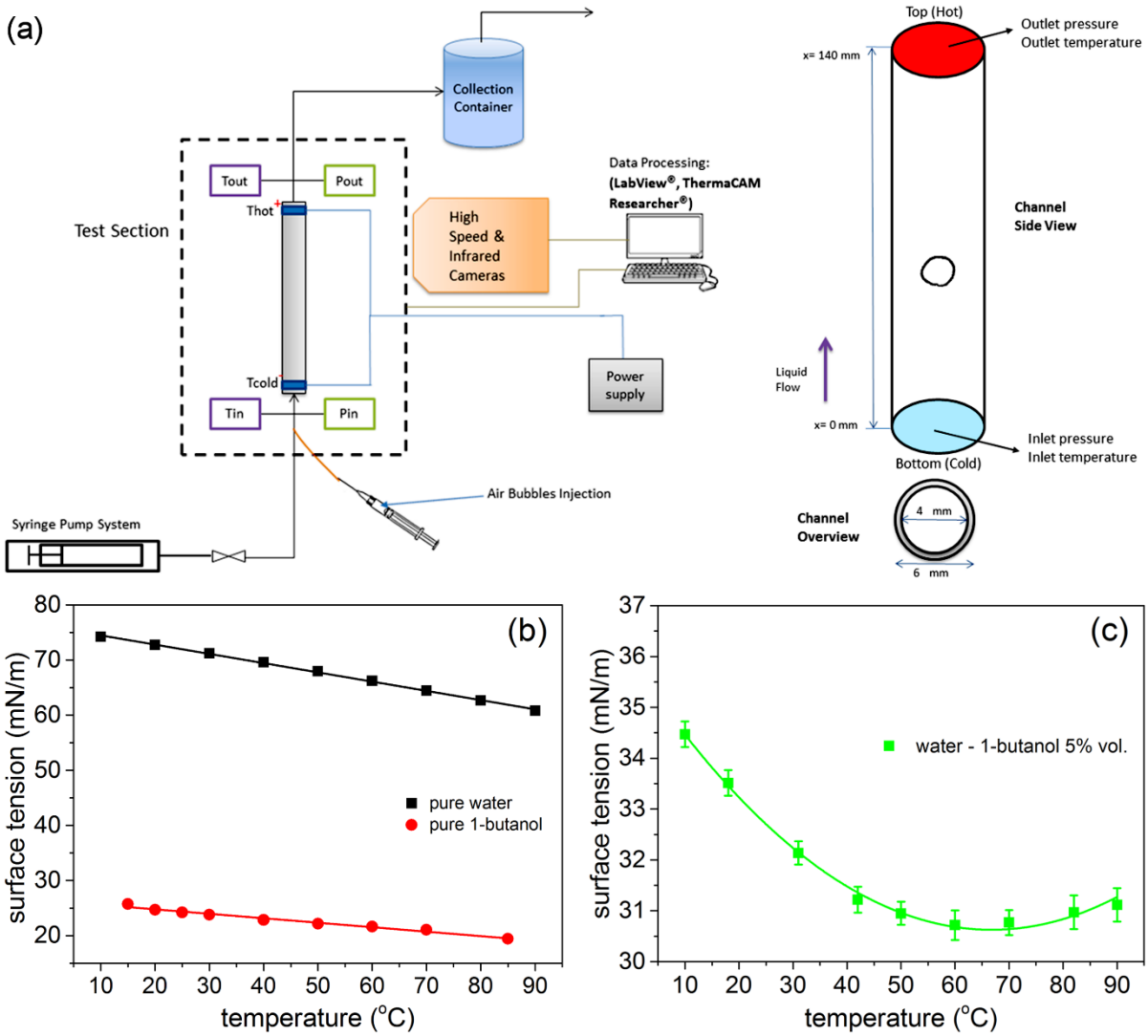

Fig. 1. (a) Schematic drawing of the experimental setup and the tested micro-channel. Surface tension measurements (mN/m) of the (b) pure liquids: pure water (■) and pure 1-butanol (●) and for the (c) self-rewetting fluid: water – 1-butanol 5% vol. (■), in the temperature range from around 10 to 90 °C, under controlled experimental conditions.

2.2. Data reduction

For the single phase flow, the effective heat, Q_{eff}, transferred to the liquid was estimated by using: $Q_{eff} = C_{p,l} \cdot (T_{out} - T_{in})\dot{m}$ where $\dot{m}$ (kg/s) is the mass flow rate, $C_{p,l}$ is the liquid specific heat capacity, T_{in} and T_{out} are the inlet and outlet liquid temperatures, respectively.

Then the heat flux was calculated as $q = Q_{eff}/A$, where A is the channel's internal surface area. For the two-phase flow, heat loss was estimated considering the convective loss Q_{conv} and the radiative loss Q_{rad}. The convective heat loss was calculated as follows: $Q_{conv} = h_{conv} \cdot A_{W,out} \cdot (T_{W,avg} - T_{env})$ where h_{conv} is the convective heat transfer coefficient of air. h_{conv} was estimated using the empirical correlations of natural convection external flow conditions at 20 ºC: $h_{conv} \sim h_{air} = Nu \cdot k/L$, where Nu is the Nusselt number, k is the thermal conductivity of air (~0.0257 W/m·K), L is the characteristic length of the channel (around 0.01 m). In addition, $T_{W,avg}$ is the average temperature of the channel wall, T_{env} is the ambient temperature and $A_{W,out}$ is the outer surface area of the tested circular micro-channel. The radiative loss was calculated by: $Q_{rad} = \varepsilon \cdot \omega \cdot A_{W,out} \cdot (T_{W,avg}^4 - T_{env}^4)$ where ε is the total emissivity of the micro-channel and its deposit, and ω is the Stefan–Boltzmann constant (5.6703×10^{-8} W/(m^2·K^4)). The emissivity of tantalum deposit on the borosilicate glass channel was found in literature (Malter and Langmuir [45], Allen *et al*. [46], Miloševic *et al*. [47]) mainly for high temperatures ranges. The emissivity ε is an increasing function of temperature and ε was reported to be 0.136 at 1000 K [45] and close to zero at around 20 ºC [47]. Thus, in the present study, tantalum emissivity ε was approximated to be 0.05 (from ~35 ºC to ~110 ºC). Actually, the calculated Q_{rad} was very low ($Q_{rad} < 1$ W) compared with the total heat Q_{eff}, thus the approximation of ε and Q_{rad} resulted in negligible errors regarding the heat loss calculations. The settings of the IR camera within the software (ThermaCAM Researcher Professional®) allowed estimation of temperature profiles along the wall channel by using some fixed parameters. These parameters which are essential for temperature measurements include the object emissivity, the object distance from the IR camera lens and the atmospheric conditions (humidity and temperature of the atmosphere). The spectral emissivity of the used borosilicate glass micro-channel (opaque object to IR radiation) and its deposit was determined experimentally according to the method by Madding [48]. The emissivity of an object is

measured by rising the target into two different and known temperatures, hence the ε can be determined as: $\varepsilon = T_{IR1} - T_{IR2}/(T_1 - T_2)$, where T_{IR1} and T_{IR2} are the infrared camera temperature measurements and T_1 and T_2 are the known measured temperatures [48]. In all the tests, emissivity fell in the range of 0.76 – 0.80, therefore a value of 0.78 was set as the channel wall emissivity [49,50]. The effective heat transferred in the two-phase flow was given by: $Q_{eff} = Q - Q_{conv} - Q_{rad}$, and the heat flux was applied on the test section was $q = Q_{eff}/A$. Each test condition was repeated ~7 times and the characteristic heat transfer profiles were obtained.

The calibration of the IR video was carried out by measuring the pixels of a known-length within the same view field. The calculation of Biot number (Bi) allowed to study the temperature uniformity within the channel body by comparing the heat conduction resistance to the heat convection resistance: $Bi = \frac{h_c d_{wall}}{k_{channel}}$, where h_c is the convective heat transfer coefficient calculated as described by Shah and London [51], d_{wall} is the channel wall thickness and $k_{channel}$ is the thermal conductivity of the channel body. Following the above mentioned, a Biot number at around ~0.06 was found in our system. Since $Bi \ll 1$, the difference between the inner and outer wall temperatures can be neglected [52]. Therefore, the channel outer surface temperature was used to calculate the local heat transfer coefficients. The thermally observed region of the channel was divided into 9 segments. Thus, the time-averaged temperatures at 9 locations (marked in Fig. 2) were calculated to study the local heat transfer coefficient, $h_{T.P.}$, in the two-phase flow, along the channel axial direction, h: $h_{T.P.} = \frac{q}{T_{W,local} - T_{l,local}}$, where $T_{W,local}$ was the local wall temperature of the microchannel and $T_{l,local}$ was the local liquid temperature in the micro-channel. $T_{l,local}$ was increased along with the flow direction. In the present study, inlet and outlet fluid temperatures were acquired by the inserted K-type thermocouples; accurate to ±0.5 ºC. The local liquid temperatures in axial

direction across the channel were not experimentally measured due to the fragility of the channel and the consequent inconvenience of thermocouple installation, which would deteriorate the transparency and damage the tantalum coated surface of the channel. The local liquid temperature was calculated based on the assumption that all the effective heat flux was used to heat up the liquid. This leads to the following energy balance: $2x \cdot d_{in} \cdot q = C_p \cdot \varphi \cdot A_c \cdot (T_{l,x} - T_{in})$ where $T_{l,x}$ (or $T_{l,local}$) was the local liquid temperature at a distance x (mm) from the channel inlet, and T_{in} was the inlet liquid temperature. So the liquid temperature can be written as: $T_{l,x} = \frac{2q \cdot d_{in}}{C_p \cdot \varphi \cdot A_c} x + T_{in}$. According to the standard uncertainty analysis of Taylor [53], the estimated maximum uncertainties are summarised in Table 1. Note that both mass fluxes and volume flow rates used are related to the liquid flow.

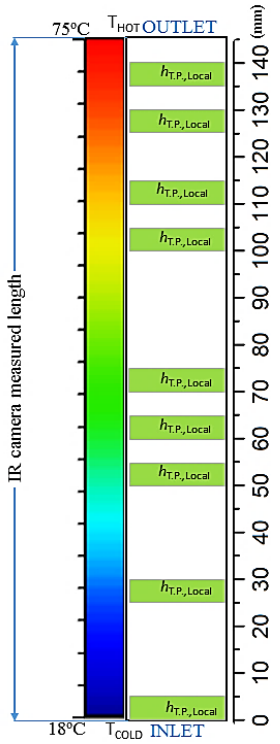

Fig. 2. Schematic drawing of the liquid temperature along the channel and the local heat transfer calculated areas.

Table 1 Experimental measurement uncertainties

Parameter	Maximum uncertainty (%)
Pump volumetric flow rate	0.5
Voltage	0.2
Current	0.5
Channel depth and thickness	10
Channel width and length	2
Infrared IR camera measured temperature	2
Channel surface area	5.5
Mass flux	10.5
Heat flux	5.5
Flow Velocity	12.5
Bubble width (diameter) and length	8.5
Bubble radius	8.5
Heat transfer coefficient	20
Local liquid temperature	17

3. Results

The use of transparent micro-channels allowed for visualization of the motion (movement and shape geometry) of the induced travelling air bubbles in a continuous liquid phase flow, before and after applying heat on a circular micro-channel. With the use of high-speed camera, different flowing patterns were observed within the micro-channel. Bubbly flow and in some specific cases slug flow were recorded depending on the applied experimental conditions and the working fluids. Different operating fluids i.e. pure water, pure 1-butanol and water – 1-butanol 5% vol., at same controlled conditions, demonstrated different bubble activity. In Fig. 3, we present a typical sequence of high speed images with bubbles flowing vertically in a

heated micro-channel containing two different working fluids: (a) pure water and (b) pure 1-butanol, versus time, at volume flow rate of $\dot{V}$ = 0.5 mL/min. In these cases, the induced bubbles were migrating from below (inlet) towards the upper part (outlet) of the channel and the temperature was increasing in the same direction. In Fig. 3(a), the migrating bubble in pure water was shown to follow steady shape geometry. In the case of the pure 1-butanol working fluid, Fig. 3(b), the bubble geometry appeared slightly to fluctuate, adopting a disk-like shape rather than spherical shape, at $\dot{V}$= 0.5 mL/min.

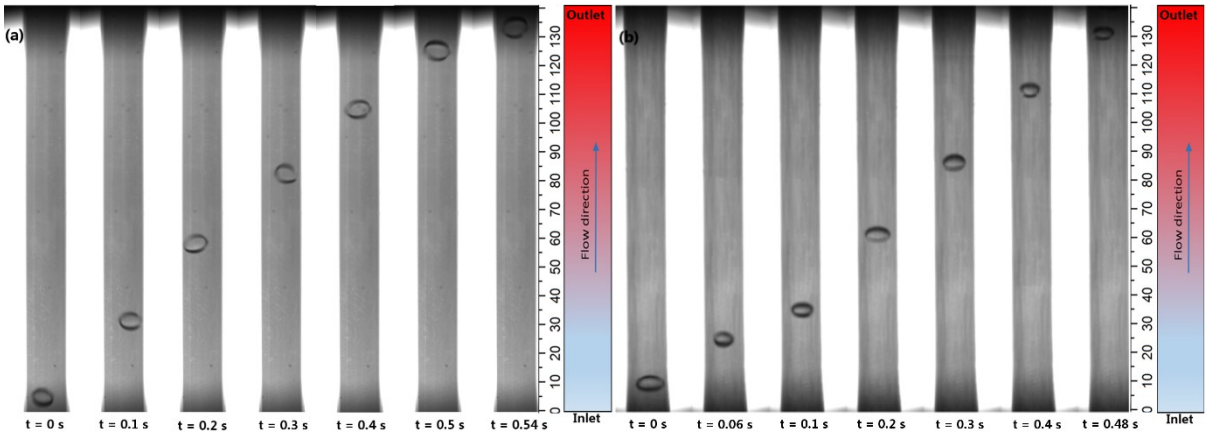

Fig. 3. Typical image sequence of the induced travelling air bubbles along the (vertical) heated micro-channel, against time. Images depict bubble travelling in (a) pure water; bubble diameter (width): ~2.2 – 2.5 mm, and (b) pure 1-butanol; bubble diameter (width): ~2.0 – 3.1 mm, at volume flow rate of $\dot{V}$ = = 0.5 mL/min, in a temperature gradient field from ~18 ºC to ~75 ºC, respectively.

In Fig. 4, we present subsequent images of migrating bubbles in the water – 1-butanol 5% vol. mixture, versus time, at four different volume flow rates ($\dot{V}$ = 0.2, 0.5, 1, 1.5 mL/min), in the same controlled temperature gradient field (~18 ºC to ~75 ºC), respectively. It can be seen that different flow patterns were observed depending on the applied volume flow rates, in the binary alcohol mixture. Initially, at $\dot{V}$ = 0.2 mL/min, Fig. 5(a), bubbly flow was observed, then it

changed to slug flow and within some seconds back again to bubbly flow just before the bubble reached the outlet side of the channel. Interestingly, at flow rate of 0.5 mL/min, Fig. 4(b), the migrating bubble was shown to behave differently and a characteristic increase in bubble size was clearly observed in the neighbourhood of the surface tension minimum and close to the outlet part of the heated channel. The same phenomenon but with a lower bubble growth can be seen at $\dot{V}$ = 1 mL/min, Fig. 4(c). On the contrary, bubble size was not affected at flow rate of 1.5 mL/min in the alcohol mixture, Fig. 4(d); the bubble followed steady geometry without visible fluctuations in size. It is clear that at different volume flow rates in the mixture and in the same temperature gradient field, the induced travelling bubbles behaved differently; hence altering the heat transfer profile in the micro-channel.

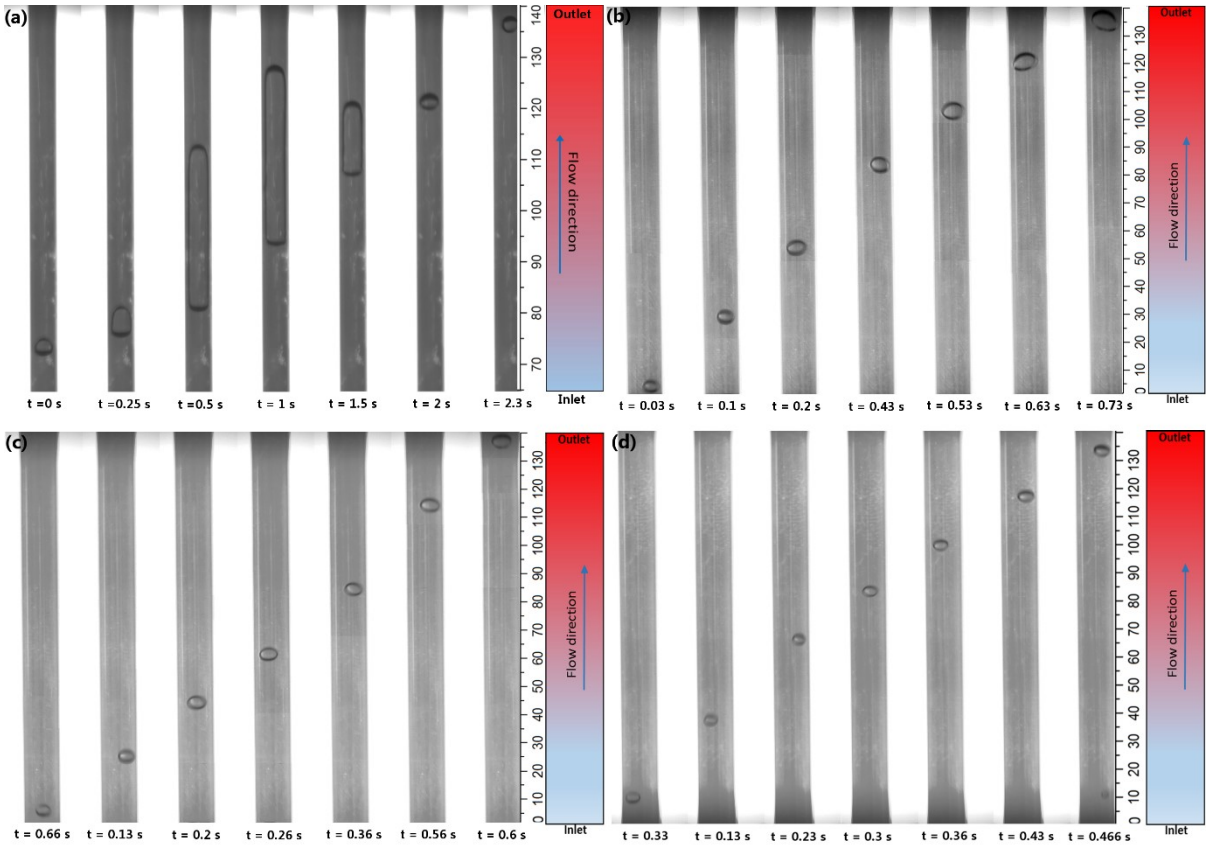

Fig. 4. Visualisations of the induced travelling air bubbles (initial diameter: from ~1.9 to 2.1 mm) along the (vertical) heated micro-channel containing water – 1-butanol 5% vol. mixture, versus time. Bubbles are flowing vertically in the binary alcohol mixture following the fluid flow, at four different flow rates, $\dot{V}$: (a) 0.2, (b) 0.5, (c) 1 and (d) 1.5 mL/min, in the same temperature gradient field, from from ~18 to ~75 ^{o}C, respectively. Note that in the image (a), the observed bubbly-slug-bubbly behaviour started at ~73 mm from channel's inlet side until locations close to the outlet where the change in the flow mode occurred.

In Fig. 5, we present results of the bubbles position, x, travelling in pure water and in pure 1-butanol along the circular micro-channel, versus time, at three different volumetric flow rates i.e. $\dot{V}$ = 0.5, 1 and 1.5 mL/min, respectively. The data in Fig. 5 (a) and (b) show the migration of the manually induced air bubbles under isothermal conditions, at constant temperature of ~18 ^{o}C, with the characteristic velocities, v, acquired from the experimental analysis of the bubbles motion. Graphs (c) and (d) depict the non-isothermal cases for the pure liquids, where the bubbles travelled from the cold side (bottom of the channel) to the hot side (top of the channel) in a controlled temperature gradient field from ~18 to ~75 ^{o}C. The characteristic velocities presented in Fig. 5 were obtained after a linear fitting for each case. It is clear from the obtained results for the pure liquids that the bubbles travelled for longer time-period in the non-isothermal cases compared to those in the isothermal ones.

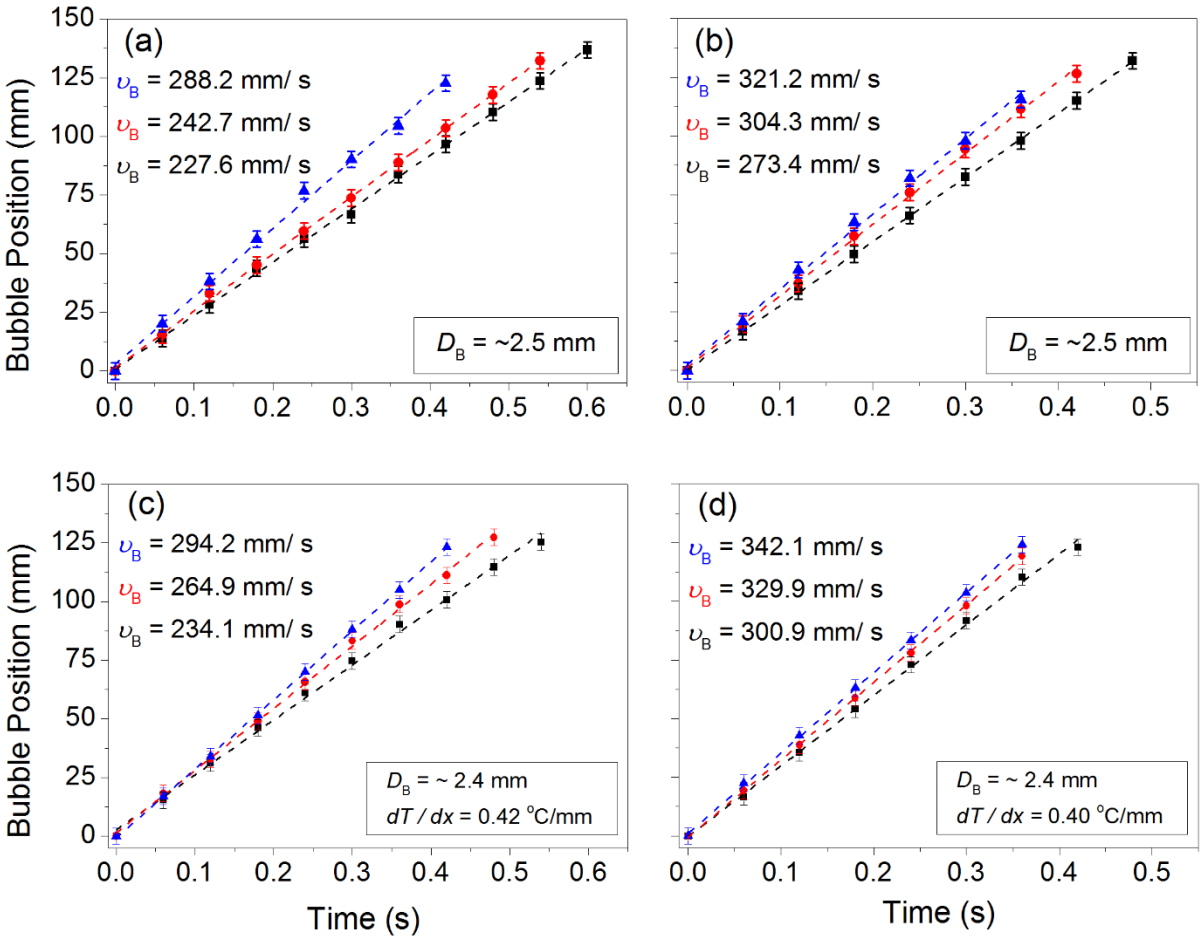

Fig. 5. Examples of the air bubbles positon, x, along the circular channel in pure water and pure 1-butanol, both in isothermal and temperature gradients cases, at $\dot{V}$: 0.5 (■), 1 (●), 1.5 (▲) mL/min, against time. More specifically, graphs (a) pure water and (b) pure 1-butanol depict calculations for the isothermal case, at temperature of ~18 °C, and with the characteristic velocities, υ, for each flow rate. Graphs (c) and (d) present examples of migrating bubbles (initial D_B = ~2.4 mm) in pure water and 1-butanol, respectively, in temperature field, from ~18 to ~75 °C and the obtained bubble velocities, υ, for each flow rate. Note that in all cases, the velocities were obtained after a linear fitting.

In Fig. 6, we show results of the air bubbles position, x, travelling in the circular micro-channel containing water – 1-butanol 5% vol. mixture, against time, at three different volumetric flow rates, $\dot{V}$: 0.5, 1 and 1.5 mL/min. Fig. 6(a) depicts data for the isothermal case, at liquid temperature of ~18 °C, with the measured characteristic velocities of the vertically migrating

bubbles from the inlet to the outlet of the channel, for each flow rate. Additionally, in Fig. 6(b) we present results of the bubbles movement in the alcohol mixture, from the gold (inlet) to the hot side (outlet) in a temperature gradient field (~18 to ~75 ºC), versus time, at the same three volume flow rates as discussed above. It is worth noting that in all cases bubble velocities, υ, were estimated by using linear fitting with an exception of the two cases at $\dot{V}$: 0.5 and 1 mL/min, Fig. 6(b). In these remarkable cases, the bubbles were seen to flow non-linearly (logarithmic behaviour) along the channel and the acquired bubbles velocities are the average speeds, $\bar{\upsilon}$. Another feature is that in the non-isothermal case the bubbles were travelling for longer time-period in the mixture compared with those in the isothermal case. This point out the importance of the thermocapillary forces acting at the interface of the bubbles. The complicated behaviour of the migrating bubbles along the heated micro-channel is clearly associated with the anomalous (non-linear) dependence of the surface tension with the temperature of this binary alcohol mixture and it will be explained in the discussion chapter.

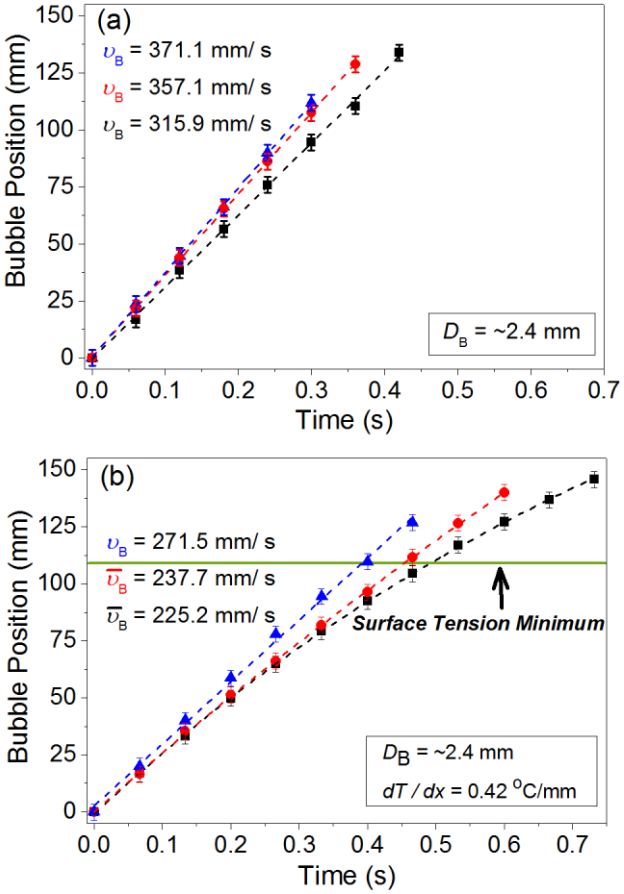

Fig. 6. Examples of the induced air bubbles position, x, along the channel in water - 1-butanol 5% vol., versus time, both in isothermal and temperature gradient cases, for three different volumetric flow rates, $\dot{V}$: 0.5 (■), 1 (●), 1.5 (▲) mL/min. More specifically, graph (a) depicts results in the isothermal case, at liquid temperature of ~18 ºC, and with the calculated velocities, υ, for each flow rate. In graph (b) the data shows bubbles in the binary mixture, with temperature gradient, from ~18 ºC to ~75 ºC, versus time, for each volume flow rate, respectively. Note that in graph (b) at $\dot{V}$: 0.5 (■) and 1 (●) mL/min, the average velocities $\bar{\upsilon}$, for each case, were obtained as the behaviour is non-linear (logarithmic shape).

In Fig. 7(a), we plot the distance, x, of the travelling bubble-slug shown in Fig. 4(a) against time and temperature. In contrast to all examples presented above (in pure liquids and in binary mixture), for this case (mixture flowing at $\dot{V}$ = 0.2 mL/min), a rather different picture was revealed regarding the migrating bubble behaviour. At the beginning, the bubble had a diameter

(width) of ~2.1 mm and was flowing upwards in the mixture. At around ~77 mm from the channel's inlet the bubble increased significantly in size and reached a width of ~3.7 mm, which is close to the channel's diameter, 4 mm; hence slug flow occurred. At the vicinity of the outlet part of channel, the fluid flow was changed back to bubbly. Fig. 7(b) presents the velocity profile of this characteristic case versus time. During the slug flow, we analysed individually the velocity profiles of the bottom (tail) and the upper part (tip) of the slug, as displayed in Fig. 7(b). It can be seen that the two sides of the slug were flowing with different velocities associated clearly with the position of the surface tension minimum along the heated channel. The velocity profile in this case was rather complex and some quantitative evaluation and comments on these results are necessary, and will be given below.

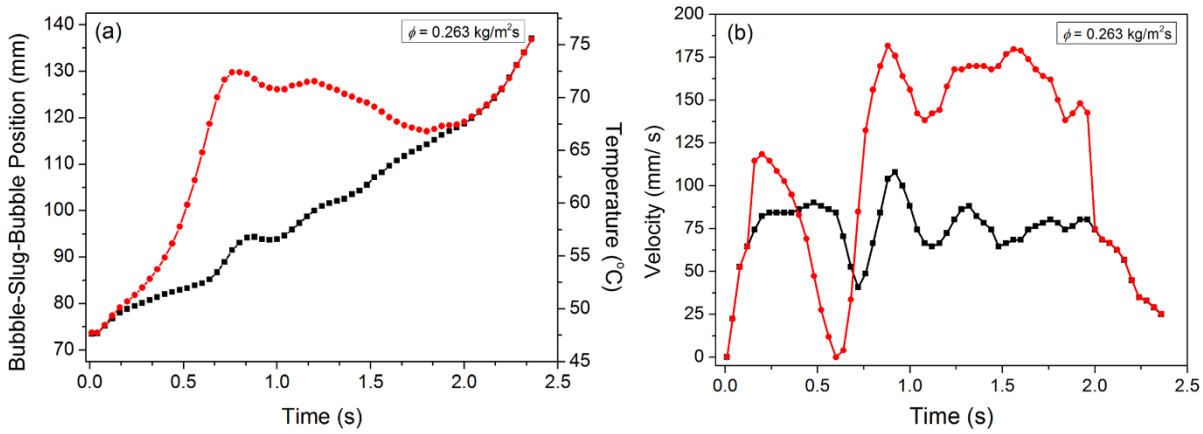

Fig. 7. (a) Portrayed behaviour (■) bottom side and (●) upper side of the bubble, shown in Fig. 4(a), of the observed bubbly-slug-bubbly flow as distance, x, at ~73 mm from inlet (cold) to outlet (hot) side of the channel versus time and temperature, at 0.2 mL/min volume flow rate. Graph (b) shows the velocity profile versus time, along the channel where (■) is velocity of the bottom (tail) and (●) is velocity of the upper (tip) side of the slug.

In what follows, we focus on the bubble geometry evolution under different experimental conditions. The travelling bubbles aspect ratios (bubble width-diameter / length) were visually measured along the micro-channel containing the pure liquids and the binary alcohol mixture, both in isothermal and non-isothermal cases. In Fig. 8 and 9, we present the aspect ratio measurements of the induced travelling air bubbles along the micro-channel in pure water (Fig. 8) and in pure 1-butanol (Fig. 9), versus time, and the position, x, at three different mass fluxes, ϕ, and average heat fluxes, q_{avg}, respectively. More specifically, in Fig. 8 the graphs (a) – (c) depict the bubble aspect ratios in the isothermal case (~18 ^{o}C) for pure water, and graphs (d) – (e) show the temperature gradient cases (from ~18 to ~75 ^{o}C), with the obtained averages (green) curve, respectively. Similarly, in Fig. 9 (a) – (c) we present bubble aspect ratio measurements in the isothermal case of pure 1-butanol as working fluid and graphs (d) – (e) depict the non-isothermal cases (from ~18 to ~75 ^{o}C), at three different mass fluxes, ϕ, and average heat fluxes, q_{avg}, respectively. Note that in the cases of the bubbles travelling in pure water, in both isothermal and temperature gradient cases, the aspect ratio values showed slight size fluctuations. Interestingly, these fluctuations were a bit stronger for the highest mass fluxes applied for these cases (as displayed in graphs (c) and (f) in Fig. 8). This might be the point that the bubbles geometry was affected by the liquid flow combined with the buoyancy effects. Similar behaviour was revealed in all the temperature gradient cases in the pure 1-butanol fluid flow where the induced travelling bubbles were seen to strongly deform and thus to fluctuate the bubbles' aspect ratios (Fig. 9, graphs (d), (e) and (f)). Note that the different physical properties (surface tension, viscosity etc.) of the operating fluids influenced the geometry of the travelling air bubbles and changed the heat transfer profile of the systems.

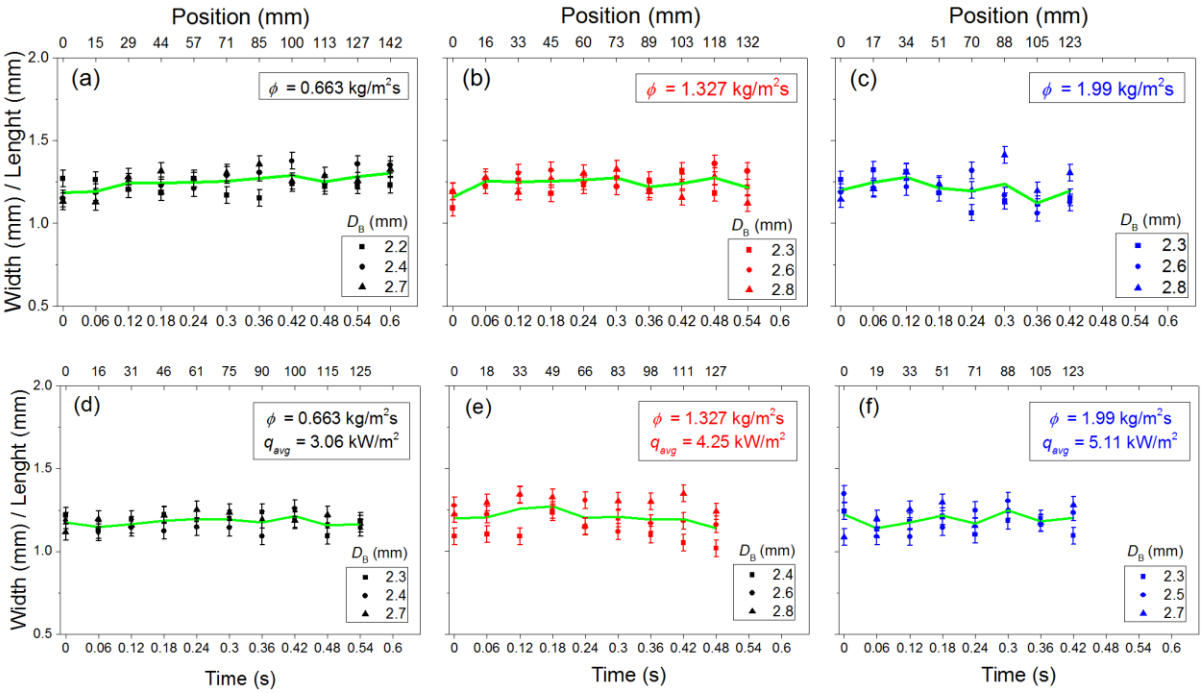

Fig. 8. Aspect ratio (bubble width / length) calculations of the migrating air bubbles along the circular microchannel in pure water (~7-fold repetitions for each case), over time, and the position, x, at three typical mass fluxes, ϕ, and at three different average heat fluxes, q_{avg}. Graphs (a) – (c) present characteristic bubble aspect ratios in the isothermal case of pure water fluid with the obtained averages (green curve), for each case. Similarly, graphs (d) – (e) show aspect ratio calculations in a temperature gradient field (~18 to ~75 ^{o}C) for three different mass fluxes, ϕ, and (average) heat fluxes, q_{avg}, respectively.

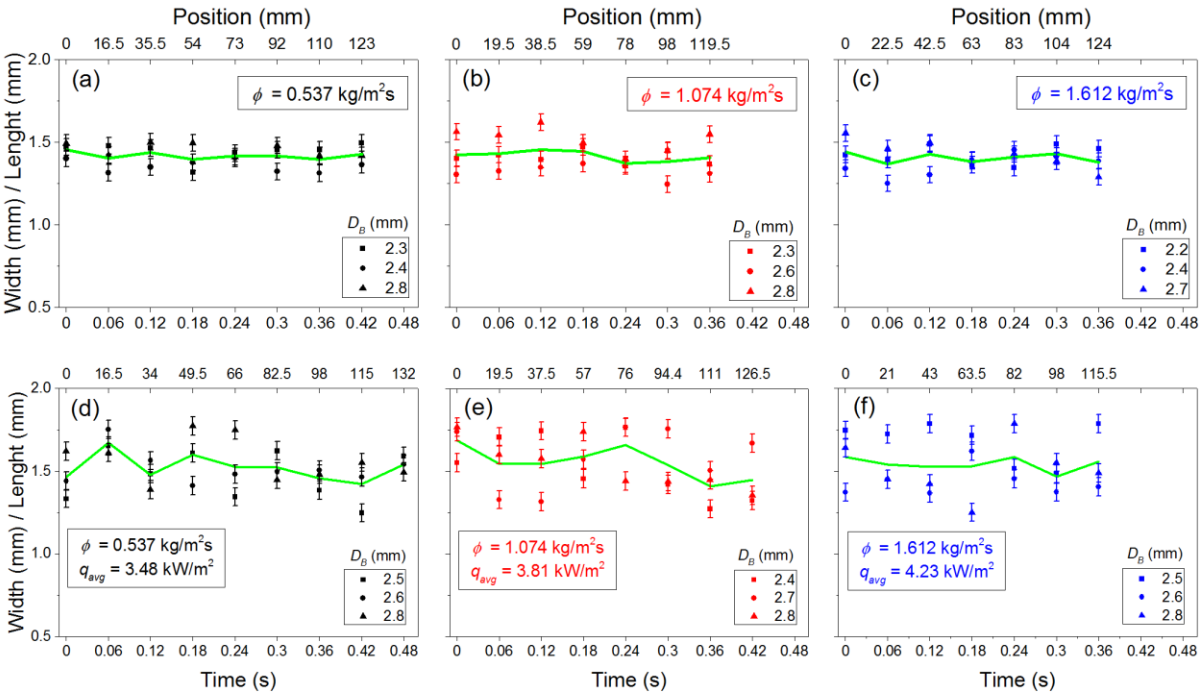

Fig. 9. Aspect ratio (bubble width / length) calculations of the migrating air bubbles along the circular micro-channel in pure 1-butanol (~7-fold repetitions for each case), against time, and the position, x, at three typical mass fluxes, ϕ, and at three different average heat fluxes, q_{avg}. More specifically, graphs (a) – (c) present characteristic bubble aspect ratios in the isothermal case of pure 1-butanol operating fluid with the obtained averages, for each case. Graphs (d) – (e) show aspect ratio values in a temperature gradient case, from ~18 to ~75 ºC, at the three typical cases.

In Fig.10, aspect ratio calculations of the induced travelling air bubbles in the water – 1-butanol 5% vol. mixture, versus time, and position, x, in the isothermal case, at ~18 ºC flowing liquid temperature, and in non-isothermal case from ~18 to ~75 ºC, at three different mass fluxes, ϕ, and average heat fluxes, q_{avg}, are presented. The graphs (a) – (c) depict aspect ratios in the isothermal cases and graphs (d) – (e) refer to the temperature gradient cases in the mixture. Interestingly, it can be seen in Fig. 10 (d) and (e) that the aspect ratio (bubble width-diameter) / length) showed a peculiar increase. A characteristic bubble ratio growth up to ~30% of the initial one was observed in graph (d), at $\dot{V}$ = 0.5 mL/min. In the case of bubble migrating at

$\dot{V}$ = 1 mL/min, an increase in bubble ratio of up to ~15% occurred. These observations are clearly associated with the anomalous (non-linear) dependence of the surface tension with the temperature for this binary alcohol mixture (self-rewetting fluid) as well as with the neighbourhood near the well-defined surface tension minimum. In contrast to the previous cases, bubbles travelling in the alcohol mixture at $\dot{V}$ = 1.5 mL/min were not influenced by the temperature gradient field due to the high mass flux applied in this case.

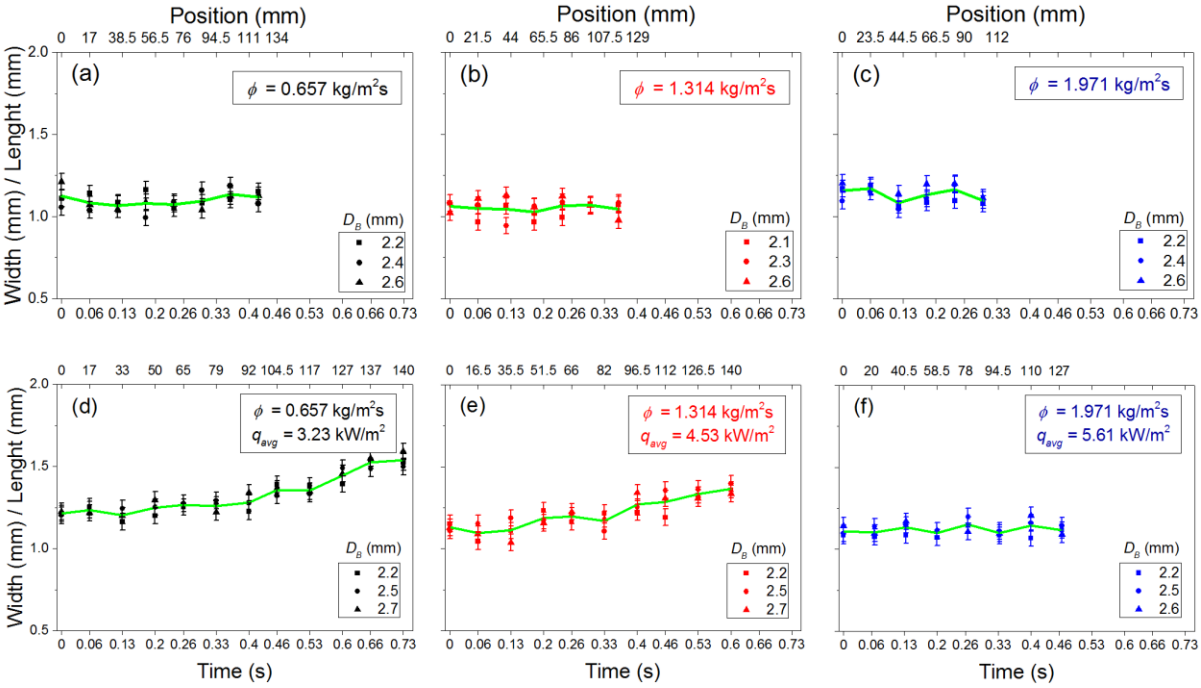

Fig. 10. Aspect ratio (bubble width / length) values of the migrating air bubbles along the circular micro-channel containing water – 1-butanol 5% vol. mixture (~7-fold repetitions for each case), over time, and position, x, at three typical mass fluxes, ϕ, and at three average heat fluxes (temperature gradient cases), q_{avg}. More specifically, graphs (a) – (c) present typical bubble aspect ratio calculations in the isothermal case with the averages, for each case, respectively. Graphs (d) – (e) show aspect ratio calculations in a temperature gradient field, from ~18 to ~75 ^{o}C, at the three different cases.

Fig. 11 presents the size (width-diameter and length) of the bubble-slug-bubble case, visually presented in Fig. 4(a), against the position, x, and temperature, in the alcohol mixture, (from ~18 ºC (inlet) to ~75 ºC (outlet)), at $\dot{V}$ = 0.2 mL/min. At around ~73 mm from the channel's inlet, the bubble showed a significant increase in length and the bubble width reached the size of the channel's diameter (~3.7 mm); then we observed the characteristic slug flow to occur (at around 77 mm). Interestingly, the slug flow was changed back to bubbly flow at ~118 mm from channel's inlet until the outlet side. The behaviour of the bubble in the alcohol mixture, at this (lowest) volume flow rate ($\dot{V}$ = 0.2 mL/min), was strongly affected by the temperature gradient field (neighbourhood of surface tension minimum; from ~55 to ~70 ºC) and the generated strong thermocapillary forces acting at the interface of the gas-liquid phases combined with the gravitational forces.

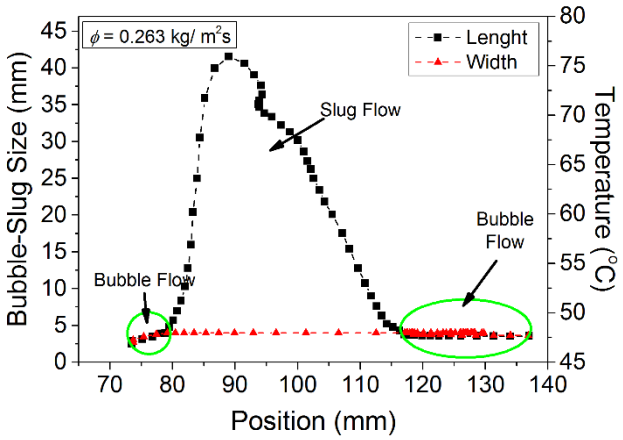

Fig. 11. Typical example of the bubble-slug-bubble case (start at ~73 mm from the channel's inlet) containing water – 1-butanol 5% vol. mixture versus the position, x, and temperature, along the heated micro-channel, at $\dot{V}$ = 0.2 ml/min liquid flow rate.

In Fig. 12, the dependency of the heat transfer coefficient, $h_{S.P.}$, in the single phase flow, on the heat flux, at ten different mass fluxes, ϕ, containing the ordinary liquids (pure water and

pure 1-butanol) and the water – 1-butanol 5% vol. mixture, in a temperature gradient field from ~18 °C (inlet) to ~75 °C (outlet), was examined. As the higher flow rate strengthens the convective heat transfer, the corresponding channel wall temperature becomes lower. Therefore, higher heat flux was required to keep uniform the temperature gradient field along the channel. It can be seen in Fig. 12 that heat transfer coefficient values were found to increase as heat flux was increased (also mass flux was increased in the same temperature gradient field) leading to a better heat transfer performance, for all the cases examined in our system.

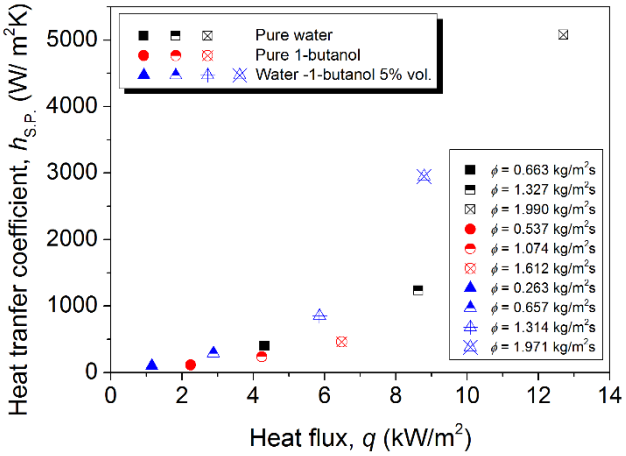

Fig. 12. Heat transfer coefficients, $h_{S.P.}$, in the single phase flow versus the heat flux, q, at ten different mass fluxes, ϕ, in the same circular heated micro-channel, for all the working fluids were used in our experimental work.

Additionally, local heat transfer coefficient calculations, $h_{T.P.}$, in the two phase flow were performed along the channel filled with the pure liquids, in a controlled temperature gradient field, ~18 – ~75 °C. Fig. 13 shows the obtained local heat transfer coefficient values of the migrating bubble in pure water, versus the position, x, and temperature, along the heated channel, at three different mass fluxes, ϕ, respectively. Moreover, Fig. 14 presents the dependency of local heat transfer coefficient, $h_{T.P.}$, in the two phase flow on the position, x,

and on temperature, containing pure 1-butanol, at three different ϕ, in the same temperature gradient field (~18 to ~75 °C). The higher mass flux used, the better the heat transfer performance was in both pure working fluid cases. Another clear feature is that the bubbles were seen to follow the same (non-linear) trend in terms of the position, x, along the channel, in the same operating fluid, but the calculated heat transfer coefficient values were higher for the higher mass fluxes, as seen in Fig. 13 and 14.

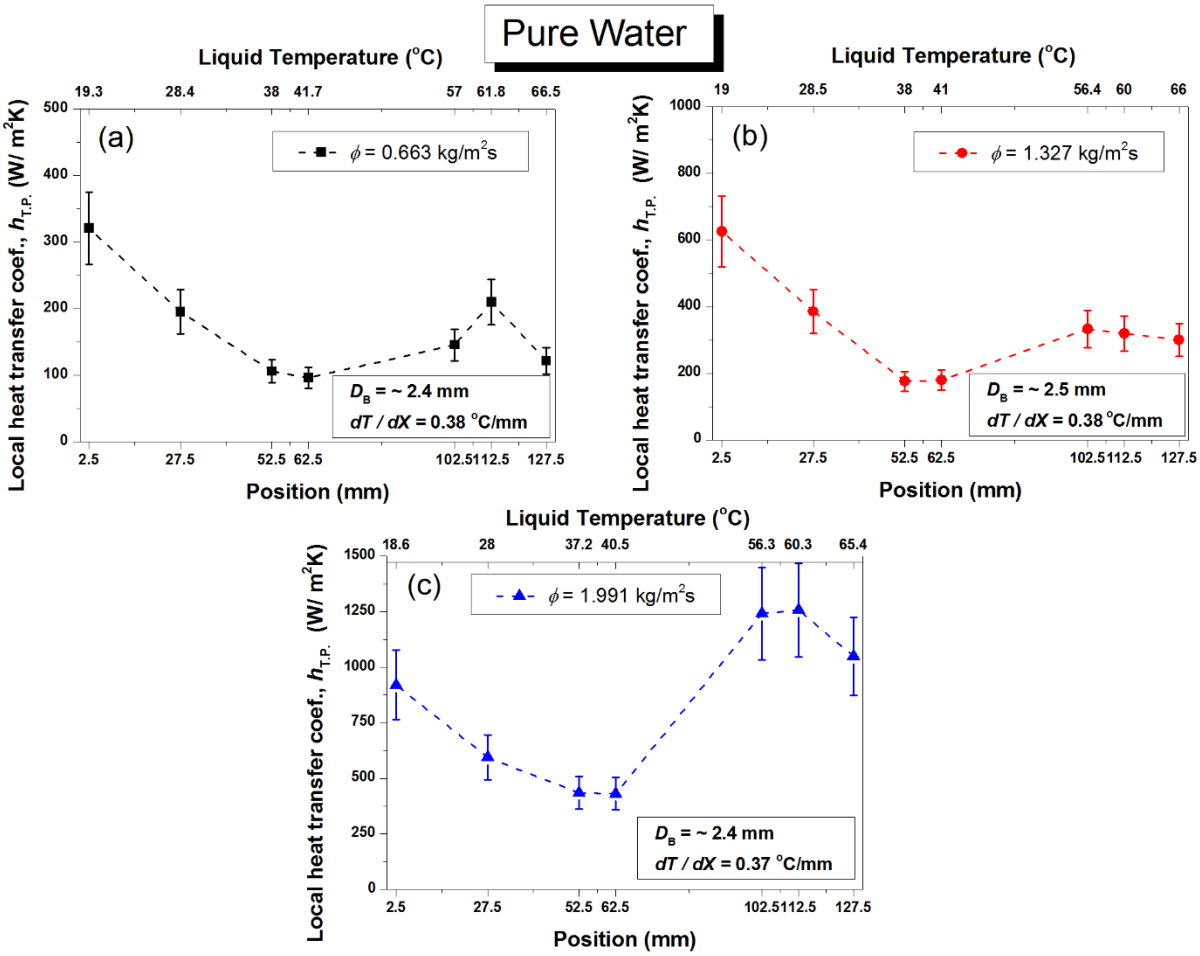

Fig. 13. Local heat transfer coefficients, $h_{T.P.}$, in the two phase flow versus the position, x, and temperature, at three different mass fluxes, ϕ, in the same temperature gradient field, from ~18 to ~75 °C, containing pure water.

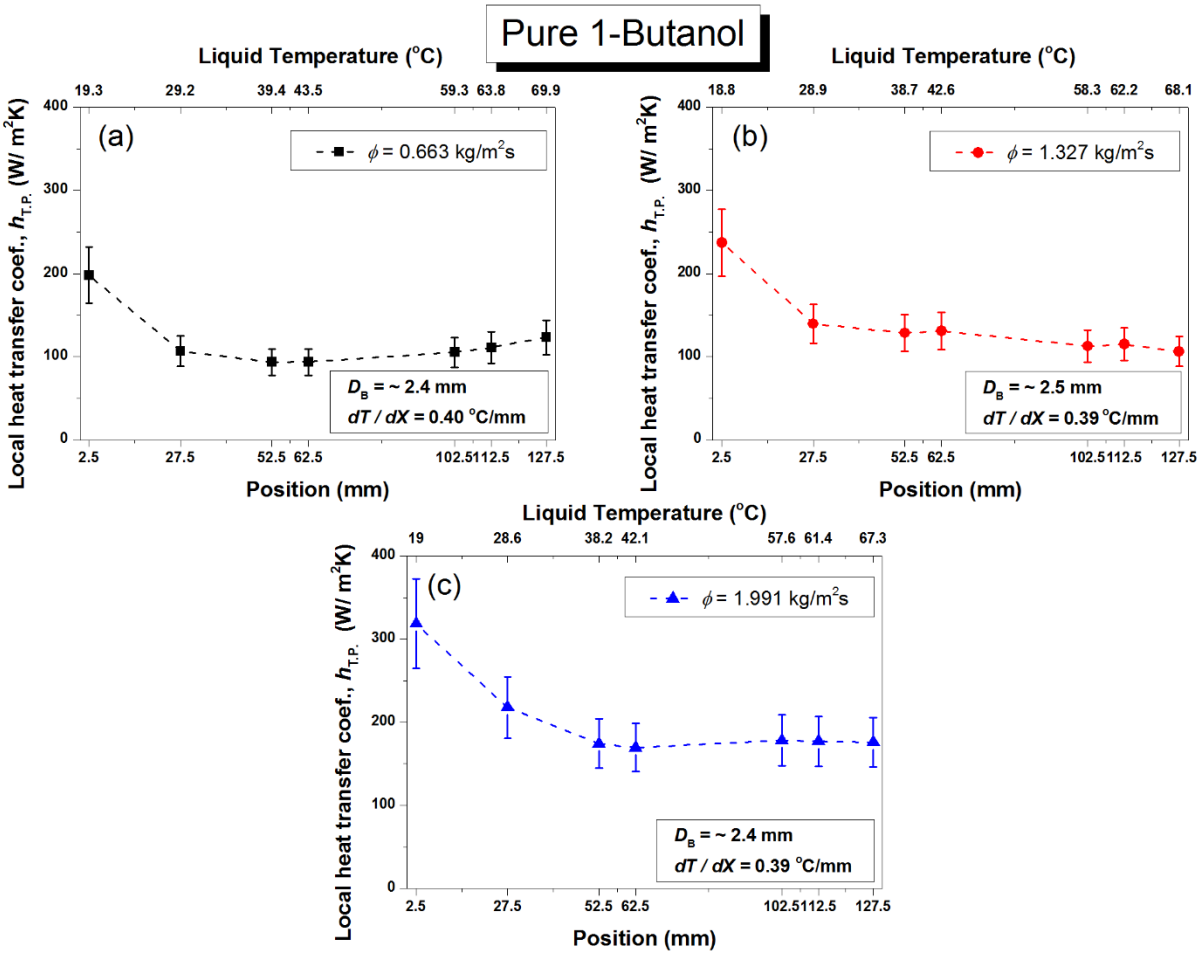

Fig. 14. Local heat transfer coefficients, $h_{T.P.}$, in the two phase flow versus the position, x, and temperature, at three different mass fluxes, ϕ, in the same temperature gradient field (~18 – ~75 °C), containing pure 1-butanol as working fluid.

Two phase flow curves of the local heat transfer coefficients, $h_{T.P.}$, of the induced travelling bubbles in water–1-butanol 5% vol. mixture as a function of the position, x, and temperature, along the circular micro-channel, at four different mass fluxes were calculated, Fig. 15. In details, graph (a) presents local heat transfer coefficients obtained in the characteristic case where the flow mode was changed from bubbly to slug and back to bubbly flow just before the outlet part of the channel, at $\dot{V}$ = 0.2 mL/min. It can be seen in graph (a) the local heat transfer coefficients increased significantly (highest $h_{T.P.}$) in the phase region where the slug occurred.

Fig. 15(b) reveals that the motion of the travelling bubble changed when the flow rate was increased in the system, at $\dot{V}$ = 0.5 mL/min. The characteristic bubble growth, as it was visually seen in Fig. 4(b) and calculated in Fig. 10(d), was accompanied by an increase in the local heat transfer coefficient values, at the higher positions of the channel. Similarly, in Fig. 15(c) the local heat transfer distribution along the heated channel was seen to follow the same tendency but with higher $h_{T.P.}$ than in the previous case. One characteristic sharp jump in the heat transfer coefficient values at temperatures around 40 ºC occurred, at the highest volume flow rate at $\dot{V}$ = 1.5 mL/min, in Fig. 15(d). Then the system was seen to follow same behaviour with the previous two cases but with higher $h_{T.P.}$ values. Moreover, comparing the calculated $h_{T.P.}$ values of the four cases in the alcohol mixture, it was seen that the highest $h_{T.P.}$ values were achieved when the highest mass flux was applied in the two-phase flow system.

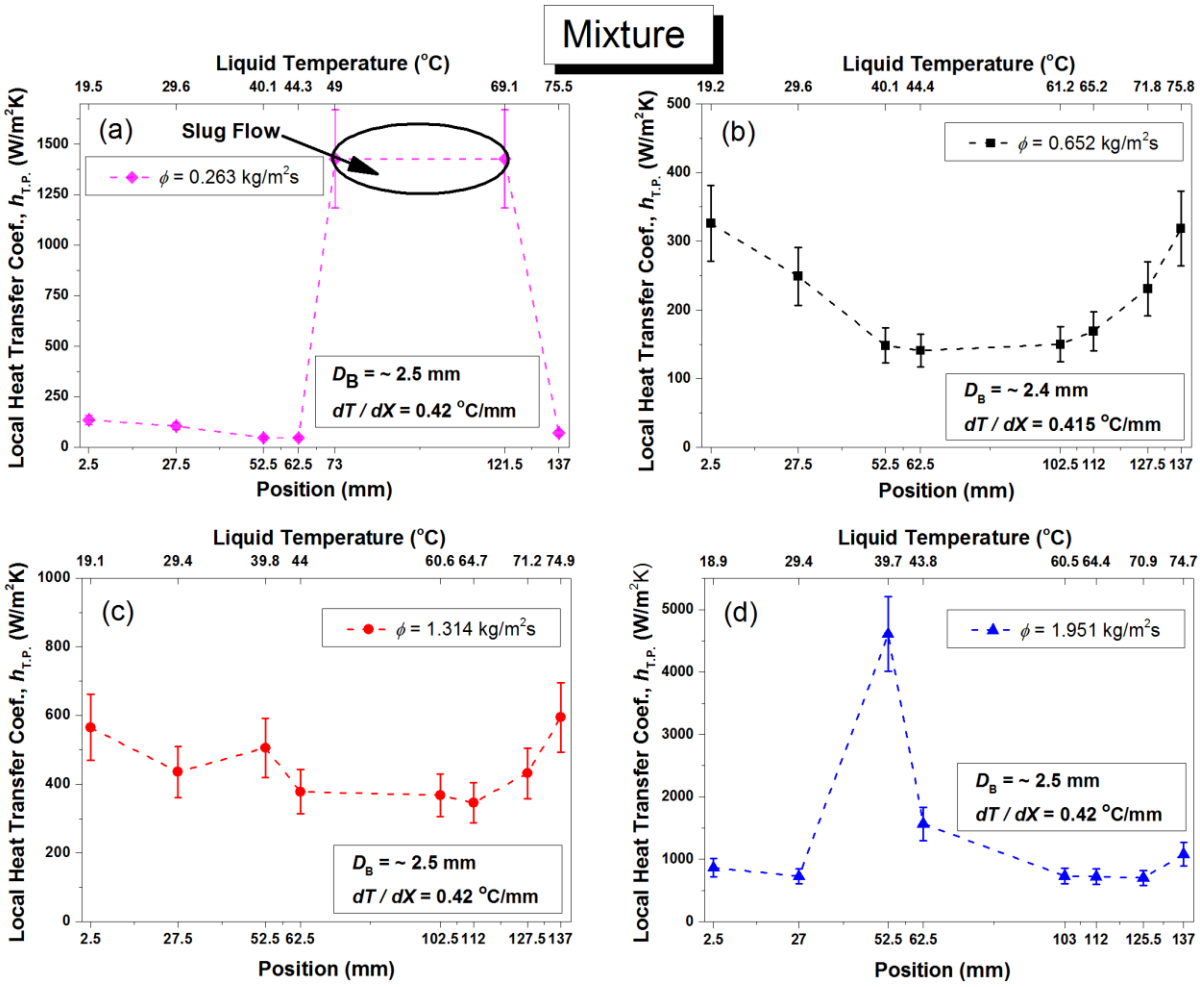

Fig. 15. Local heat transfer coefficient, $h_{T.P.}$, calculations in the two phase flow containing water – 1-butanol 5% vol. mixture versus the position, x, and temperature, at four different mass fluxes, ϕ, in the same temperature gradient field (~18 – ~75 °C), respectively.

4. Discussion

From our experimental investigation and analytical calculations, we have shown that the motion of migrating spherical bubbles along the micro-channel depends strongly on the working fluids (pure liquids and binary alcohol mixture used) and the applied experimental conditions (isothermal and non-isothermal cases). More specifically, the rising bubbles in the pure liquids followed a relatively constant linear velocity profile for both the isothermal and the non-isothermal cases (Fig. 5). Another feature, for the bubbles flowing in pure liquids was

the presence of thermocapillarity (Marangoni convection) which was driving liquid flows towards the cold regions of the channel and therefore was enhancing the upward motion of the bubble. The induced thermocapillary stresses in the linear temperature gradient field caused the bubbles to reach a higher rise velocity than in the isothermal ones, for all the mass fluxes applied and this behaviour was also attributed to the physical properties (surface tension, viscosity etc.) of the pure liquids.

Using the water – 1-butanol 5% vol. mixture as the continuous bulk liquid in a heated micro-channel, we have observed that the behaviour of the induced travelling bubbles in the binary alcohol mixture (Fig. 4) departs considerably from those of the pure liquids. The anomalous surface tension behaviour of the self-rewetting fluids, Fig. 1 (c), and the position of surface tension minimum along the uniformly heated micro-channel (Fig. 16) drastically affected the induced thermocapillary stresses. Interestingly, bubbles flowing towards the warmer zone (upstream) in the alcohol mixture within the applied temperature gradient field, induced a non-linear (logarithmic) velocity profile at $\dot{V}$: 0.5 and 1 mL/min (Fig. 6). However, the air bubbles travelling in the mixture at volume flow rate of 1.5 mL/min (highest in this work) followed a linear velocity profile as in the pure liquid cases. Remarkably, the migrating (air) bubbles in the mixture at $\dot{V}$: 0.2 mL/min (lowest used) resulted in a changing flow mode i.e. bubbly-slug-bubbly flow, adopting a highly non-linear behaviour, Fig. 7. Along the micro-channel, bubbles were influenced by three factors: the buoyancy effects, the liquid flow and the thermocapillary (Marangoni) stresses. The bubbles were clearly affected or even changed the flow mode (e.g. when slug flow occurred) inside the channel, when thermocapillarity influenced the system strongly and drove flow in the vicinity of the liquid-gas interface, in the case of the non-isothermal mixtures. The rising bubbles were subjected to (strong) interfacial forces depending on the immediate position of the bubbles in the parabolic curvature of the surface tension.

Therefore, at positions in the channel that corresponded to higher values of surface tension than its minimum, with positive gradient ($d\gamma / dT > 0$), Fig.16, the induced Marangoni stresses drove liquid upwards towards the hotter region of the channel, and inhibited the upward motion of the bubble. The reverse phenomenon occurred at positions corresponding to lower values of the surface tension minimum with a negative gradient ($d\gamma / dT < 0$, Fig. 16), hence promoting the upward movement of the bubbles. This was evident in the non-isothermal cases for the mixture, where it was shown that the rising velocity of the bubbles was lower than of those in the isothermal ones (for the three different mass fluxes). The generated strong net capillary force due to the temperature gradients (surface tension gradients) caused the bubbles migration to fluctuate and deformed their shape-geometry. This is the reason behind the non-linear retardation of the bubbles until the outlet part of the channel for the two cases at volume flow rates of 0.5 and 1 mL/min, in the non-isothermal mixture systems. However, the bubbles migrating in the alcohol mixture, at $\dot{V}$: 1.5 mL/min, followed a linear behaviour along the heated channel as the increased liquid flow (combined with the buoyancy effect) dominated over thermocapillary stresses. Our results have demonstrated that the motion of the bubbles in a self-rewetting fluid can be more complex and deviations (from the usual behaviour in pure liquids) can be attributed to the generated thermocapillary flows, which oppose or promote the direction of the buoyancy-driven bubble rise and alter the bubble geometry.

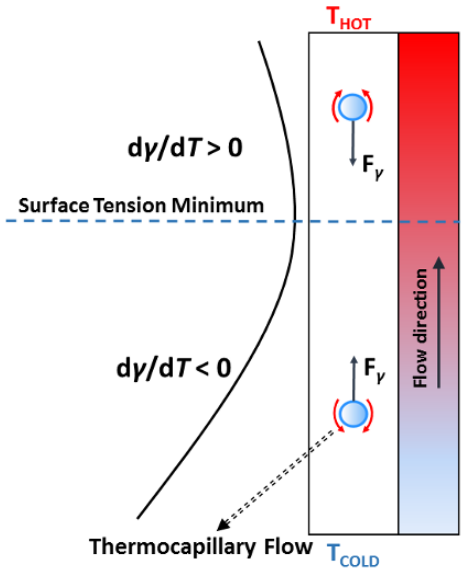

Fig. 16. Schematic drawing of the presence of Marangoni stresses acting at the interface of the migrating bubbles system. Note that at positions corresponding to lower values of the surface tension minimum, interfacial flows enhance the upward movement of the bubbles and the reverse phenomenon occurs at higher positions from the well-defined minimum.

Previous experimental and theoretical studies on the rising and deforming of a single bubble in a liquid flow have been reported in the literature [54–59]. The bubbles shape varies greatly in different flow regimes as a function of the non-dimensional parameters such as Reynolds ($Re = \dot{V} \cdot d_{in}/(\mu_l \cdot A_c)$), Rayleigh ($Ra_L = Gr_L \cdot Pr_{air}$, where Gr is the Grashof number and Pr is the Prandtl number), Nusselt ($Nu \approx 0.54\,(Ra_L)^{1/4}$), Marangoni ($Ma = -\left(\frac{d\sigma}{dT}\right) \cdot \frac{\Delta T}{\mu_l \cdot \alpha} \cdot \frac{{D_B}^2}{d_{in}}$), Capillary ($Ca = \mu_l \cdot u_l/\gamma_l$) and Bond ($Bo = \Delta\rho \cdot g \cdot {d_{in}}^2/\gamma_l$) numbers. Considering the importance and the competition between forces acting on our non-isothermal system, calculation of the dimensionless numbers for pure fluids and alcohol mixture was carried out, as seen in Table 3. Small bubbles (r = ~1.2 mm) travelling along the microchannel with relatively small Reynolds and Bond numbers ($Re < 1$ and $Bo < 1$), were seen to rise in a steady fashion, sustained the spherical shape and increased in size due to thermocapillary-

driven flows (surface tension forces variations) along the heated channel. The shape of larger bubbles, with intermediate Reynolds and Bond numbers ($1 < Re < 100$ and $1 < Bo < 100$), were affected significantly by the flow conditions and the action of buoyancy effects. In our experiments the Reynolds number were characteristically low resulting in a smooth, constant fluid flow; laminar flow. Calculations of the Rayleigh and Nusselt numbers (channel's inlet) demonstrated that the heat transfer was primarily in the form of heat (natural) convection (high Ra numbers and $Nu > 1$), in all cases. For the pure water cases, the dimensionless numbers showed that the migration of the bubbles was mainly driven by gravity, the imposed liquid flow and the thermocapillarity. The presence of strong surface tension forces maintained the spherical shape of the bubbles; Bo = 0.54 and $Ca < 10^{-5}$ i.e. capillary forces dominated in flow over viscous forces, and enhanced the upward movement along the heated channel. On the other hand, the rising bubbles in pure 1-butanol working fluid were influenced by strong body forces-buoyancy (Bo = 1.42 and $Ca < 10^{-5}$), the applied liquid flow and the weak thermocapillary stresses which was evidenced from the observations of bubble deformation and the adopted disk-like shape, Fig. 3. However, the findings presented in the self-rewetting liquid flows brought to light a new phenomenon which was first reported in the latest work of Shanahan and Sefiane [39] in which the rising bubbles migrated against the liquid flow (horizontal micro-channel) due to the strong action of thermocapillarity. In our study, air bubbles travelling in self-rewetting fluid (vertical micro-channel) were seen to be drastically influenced by the presence of strong surface tension forces (Marangoni stresses), the subjected buoyancy effects and the liquid flow. The bubbles kept a spherical shape, Bo = 0.54, and affected by the capillary action over viscous ones; $Ca < 10^{-5}$. However, it is also clear that the bubbles motion within the channel was related significantly to the position-temperature and the surface tension minimum, along the channel where either promoted or retarded the bubble movement resulting in a non-linear velocity profile (logarithmic), as reported previously [39].

The calculated Marangoni numbers (Table 3) showed that the (thermal) surface tension forces acting at the gas-liquid interface were enhanced as the bubbles were travelling in the increasing temperature gradient field, for all cases examined. Furthermore, the higher volume flow rate applied in the system the smaller the contribution of the surface tension forces (and lower Marangoni numbers) as the heat transfer rate was enhanced in the two-phase flow cases. However, it worthwhile noting that in the pure butanol liquid flows the calculated Marangoni numbers were very low ($Ma \ll 1$) indicating the strong contribution of the viscous forces (and capillary motion) in the liquid flow over surface tension forces.

The aforementioned observations about bubbles motion in the non-isothermal liquid flows were consistent with the single phase and two phase flows local heat transfer coefficients, as presented in Fig. 12-15. It was seen that for the pure liquids heat transfer coefficient curves were influenced by the mass flux in both single phase and two-phase regions. Moreover, heat transfer coefficients were sensitive to the applied heat flux in the single-phase flows and an enhancement in the heat transfer profile was calculated as the heat flux was increased, for all working fluids used. In the two-phase flows, the calculated local heat transfer coefficients were shown to follow a non-linear trend in terms of the position, and temperature, along the channel, in each flow rate, for all operating fluids. In our case, the laminar flow consists of a regular-flow pattern with constant-flow velocity throughout the liquid fluid volume and it is characterised by the flow of a fluid in parallel layers. Each layer flows at a different velocity along the same direction and the speed tended to zero near the channel's wall(s). Although, in pure water, initially the bubbles were spherical i.e. diameter-width (D_B) $\leq$ capillary length ($\lambda_c = \sqrt{\gamma/\rho g}$) *ca.* ~1.9 – 2.4 mm, they were of dimensions comparable to the channel depth. Thus, (viscous) drag was greater than that expected, due to the proximity of the channel wall(s) and even more intensive as the bubble were flowing in hotter regions of the channel (surface tension decreased). The spikes appeared in the heat transfer coefficients calculations (Fig. 13)

were attributed to the possible bubble dragging on the channel wall(s) that affected the rate of heat transfer in the system. An alternative (or additional) explanation could be a potential dry-out near the wall (induced by an enhanced shear) where the bubble is confined, resulting in a local contact line and hence high local evaporation. However, in the pure butanol flows, the air bubbles were travelling relatively faster (Fig. 5) than those of the water ones due to its different physical properties. The bubbles adopted a disc-like fluctuated shape ($D_B > \lambda_c$ *ca.* ~3 mm) and they were drastically affected by the liquid flow. Moreover, the anomalous property of the alcohol mixture, which essentially influenced the motion of the rising bubbles, was also revealed in the local heat transfer coefficient values in the two-phase flows regions. In the mixture cases, at low flow rate of 0.2 mL/min, bubble motion was apparently governed by strong thermocapillary stresses coupled with local evaporation and slug flow occurred, at the neighbourhood of the minimum of the surface tension i.e. from around ~55 to ~70 ºC, Fig. 1 (c), enhancing drastically the heat transfer profile of the system, as seen in Fig.15. The elongation of the bubble around the minimum of surface tension followed by shrinkage seems to indicate a reversal in thermocapillary stresses as the minimum location is crossed. The observations shown in Figure 4 clearly indicate a peculiar behaviour at the lowest of flow rates investigated, Figure 4(a). Whilst bubbles at higher flow rates remain relatively unconfined (size of bubbles smaller than channel diameter), Figure 4 (b), (c) and (d), at the lowest flow rate, Figure 4(a), the bubble grew to reach the diameter of the channel forming a slug which expanded and then shrank to its original size. It is worth noting that the timescale for residence time of bubble varies for different flow rates. This is of the order of 0.4 sec, 0.6 sec and 0.7 sec for higher flow rates. Whereas it is of the order of 2.3 sec for the lowest flow rate. The increased residence time of the bubble within the channel for the lowest flow rate could have led to a pronounced evaporation which could be negligible in the case of shorter residence times at higher flow rates. At the lowest flow rate in Figure 4(a), the bubble grew to be confined by the

channel wall, this amplified evaporation even further as there is a formation of a thin liquid layer on the wall. This amplified evaporation and growth of the bubble becomes more pronounced as it reached the minimum in surface tension where thermocapillary stresses pull on the bubble in opposite directions and tend to elongate the bubble further. This peculiar behaviour is believed to be a combination of enhanced evaporation because of confinement which has been caused by higher residence time, coupled with thermocapillary stress. The bubble seems to shrink after passing the minimum in surface tension point, which is probably caused by a condensation. The growth of an elongation of the bubble is thought to be a local phenomenon caused by enhanced evaporation coupled with a minimum in thermocapillary stress. Once the coupling between the two phenomena is passed, the bubble undergoes condensation and shrinks. However, at 0.5 mL/min, the local heat transfer coefficient values started to increase (again) in the proximity of the surface tension minimum until the outlet of the channel, consistent with the observed bubble ratio growth (up to ~30%). Thus, the enhancement of the heat transfer mechanism occurred at the higher position of the channel where the bubble motion was affected strongly by thermocapillarity. The same feature but less intensive (bubble ratio growth up to ~15%) was revealed at 1 mL/min, where the calculated local heat transfer coefficients increased as the bubble was flowing in the neighbourhood of the surface tension minimum (~63 ^{o}C) until the outlet of the channel. In this case, the competition between the liquid flow and buoyancy against the Marangoni stresses was more balanced and the bubbles followed an intermediate behaviour. At 1.5 mL/min flow rate, the highest local heat transfer coefficient values obtained, were associated with the highest mass flux (heat flux) applied and without bubble deformation to occur. It is worth noting that in all cases containing the alcohol mixture, different bubble motions were observed when the mass flux (and so the heat flux) in the same temperature field was altered, resulting in a different heat transfer profile. It is clear from all the above mentioned that the thermocapillarity played

an important role as an energy transport mechanism and had a major impact in the heat transfer performance of the self-rewetting systems.

Table 3 Calculated dimensionless groups for the pure liquids and water – 1-butanol 5% vol. mixture.

Liquid	Mass flux ($\frac{kg}{m^2 s}$)	Reynolds number (Re) (inlet – outlet)	Dimensionless numbers				
			Rayleigh (Ra) (inlet)	Nusselt (Nu) (inlet)	Marangoni (Ma) (inlet – outlet)	Capillary (Ca) (inlet)	Bond (Bo) (inlet)
Pure water	0.67	2.3 – 6.4	2.23 x 10^5	12.8	11.2 – 104	9.07 x 10^{-6}	0.54 (bubble flow, r_B = 1.2 mm)
	1.33	4.6 – 12.8	2.61 x 10^5	12.2	9.1 – 70	1.81 x 10^{-5}	
	1.99	6.9 – 19.2	2.25 x 10^5	11.8	5.6 – 30	2.71 x 10^{-5}	
Pure 1-butanol	0.54	0.7 – 2.4	3.67 x 10^4	8.2	0.1 – 0.5	8.98 x 10^{-7}	1.45 (bubble flow, r_B = 1.2 mm)
	1.07	1.4 – 4.8	3.3 x 10^4	7.9	0.07 – 0.45	1.79 x 10^{-6}	
	1.61	2.1 – 7.2	2.75 x 10^4	7.6	0.05 – 0.42	2.71 x 10^{-6}	
Water – 1-butanol 5% vol.	0.26	0.7 – 1.9	2.5 x 10^5	12.1	12 – 76 (bubble flow)	1.10 x 10^{-5}	0.45 (initial bubble flow, r_B = 1.2 mm) 1.11 (slug flow, r_B = 3.7 mm ≈ d_{in})
	0.65	1.8 – 4.8	1.56 x 10^5	11.5	10 – 25	2.75 x 10^{-5}	0.45 (bubble case, r_B = 1.2 mm)
	1.30	3.7 – 9.6	1.21 x 10^5	10.5	7.5 – 17	5.50 x 10^{-5}	
	1.95	5.5 – 14.4	1.13 x 10^5	10.8	5.5 – 12	8.24 x 10^{-5}	

5. Conclusions

We have carried out an experimental investigation of an air bubble rising in a non-isothermal liquid flow in a circular micro-channel whose walls have a linearly increasing temperature gradient. Particular interest was paid to the development of thermocapillary stresses due to surface gradients in pure liquids flows (pure water and 1-butanol) and in self-rewetting fluid flows (water – 1-butanol 5% vol.), and in turn, the bubble dynamics. Our results indicate that the motion of the bubble in the binary alcohol solution can be drastically affected by the presence of strong surface tension forces (Marangoni effect) and its parabolic dependence on temperature with a well-defined minimum. The presence of thermocapillarity found to promote or retard the upward movement of the buoyancy-driven bubble depending on the channel location associated with the surface tension minimum. We have also shown that in some remarkable cases of the self-rewetting fluid that the bubble experienced considerable elongation and the flow changed from bubbly to slug. This phenomenon is due to the interfacial flows acting on the travelling bubble (strong Marangoni convection), and the characteristic slow liquid flow used in this case. These motions were absent in the case of pure liquids whose surface tension decreases linearly with increasing temperature. The anomalous property of the self-rewetting fluids and the action of thermocapillary driven flows were also the key factors of the enhanced heat transfer rates compared with that of the linear liquids. The present findings highlight the importance of the Marangoni effect in two-phase flows systems linked with other phenomena such as gravitational or capillary forces.

Acknowledgments

This work was carried out under the umbrella of COST ActionMP1106: “Smart and green interfaces – from single bubbles and drops to industrial, environmental and biomedical

applications". We acknowledge funding from the Engineering and Physical Sciences Council (EPSRC) DTA.

References

[1] A. A. Bühlmann, Decompression — Decompression Sickness, Springer-Verlag Berlin New York, 1984.

[2] S. Degaleesan, M. Dudukovic, Y. Pan, Experimental study of gas-induced liquid-flow structures in bubble columns, AIChE J. 47 (2001) 1913–1931. doi:10.1002/aic.690470904.

[3] N. Kantarci, F. Borak, K.O. Ulgen, Bubble column reactors, Process Biochem. 40 (2005) 2263–2283. doi:10.1016/j.procbio.2004.10.004.

[4] T. Nowadzky, A. Pantoja, J.R. Britton, Bubble Continuous Positive Airway Pressure, A Potentially Better Practice, Reduces the Use of Mechanical Ventilation Among Very Low Birth Weight Infants With Respiratory Distress Syndrome, Pediatrics. 123 (2009).

[5] E. Livak-Dahl, I. Sinn, M. Burns, Microfluidic Chemical Analysis Systems, Annu. Rev. Chem. Biomol. Eng. 2 (2011) 325–353. doi:10.1146/annurev-chembioeng-061010-114215.

[6] N.O. Young, J.S. Goldstein, M.J. Block, The motion of bubbles in a vertical temperature gradient, J. Fluid Mech. 6 (1959) 350. doi:10.1017/S0022112059000684.

[7] R.S. Subramanian, Thermocapillary migration of bubbles and droplets, Adv. Sp. Res. 3 (1983) 145–153. doi:10.1016/0273-1177(83)90239-9.

[8] R. Subramanian, R. Balasubramaniam, N. Clark, Motion of Bubbles and Drops in Reduced Gravity, Appl. Mech. Rev. 55 (2002) B56. doi:10.1115/1.1470685.

[9] S.W.J. Welch, Transient Thermocapillary Migration of Deformable Bubbles, J. Colloid Interface Sci. 208 (1998) 500–508. doi:10.1006/jcis.1998.5883.

[10] S.K. Wilson, The effect of an axial temperature gradient on the steady motion of a large droplet in a tube, J. Eng. Math. 29 (1995) 205–217. doi:10.1007/BF00042854.

[11] A. Mazouchi, G.M. Homsy, Thermocapillary migration of long bubbles in polygonal tubes. I. Theory, Phys. Fluids. 13 (2001) 1594–1600. doi:10.1063/1.1369604.

[12] E. Lajeunesse, G.M. Homsy, Thermocapillary migration of long bubbles in polygonal tubes. II. Experiments, Phys. Fluids. 15 (2003) 308–314. doi:10.1063/1.1531617.

[13] S.M. O'Shaughnessy, A.J. Robinson, Heat transfer near an isolated hemispherical gas bubble: The combined influence of thermocapillarity and buoyancy, Int. J. Heat Mass Transf. 62 (2013) 422–434. doi:10.1016/j.ijheatmasstransfer.2013.02.064.

[14] D. Mamalis, V. Koutsos, K. Sefiane, On the motion of a sessile drop on an incline: Effect of non-monotonic thermocapillary stresses, Appl. Phys. Lett. 109 (2016) 231601.

doi:10.1063/1.4971396.

[15] M.K. Tripathi, K.C. Sahu, G. Karapetsas, K. Sefiane, O.K. Matar, Non-isothermal bubble rise: non-monotonic dependence of surface tension on temperature, J. Fluid Mech. 763 (2015) 82–108. doi:10.1017/jfm.2014.659.

[16] C. Buffone, K. Sefiane, C. Minetti, D. Mamalis, Standing wave in evaporating meniscus detected by infrared thermography, Appl. Phys. Lett. 107 (2015) 41606. doi:10.1063/1.4927744.

[17] P.T. Brady, M. Herrmann, J.M. Lopez, Confined thermocapillary motion of a three-dimensional deformable drop, Phys. Fluids. 23 (2011) 22101. doi:10.1063/1.3529442.

[18] G. Karapetsas, K.C. Sahu, K. Sefiane, O.K. Matar, Thermocapillary-driven motion of a sessile drop: effect of non-monotonic dependence of surface tension on temperature., Langmuir. 30 (2014) 4310–21. doi:10.1021/la5002682.

[19] K. Sefiane, S. David, M.E.R. Shanahan, Wetting and Evaporation of Binary Mixture Drops, J. Phys. Chem. B. 112 (2008) 11317–11323. doi:10.1021/jp8030418.

[20] K. Sefiane, L. Tadrist, M. Douglas, Experimental study of evaporating water–ethanol mixture sessile drop: influence of concentration, Int. J. Heat Mass Transf. 46 (2003) 4527–4534. doi:10.1016/S0017-9310(03)00267-9.

[21] A.K.H. Cheng, D.M. Soolaman, H.-Z. Yu, Evaporation of microdroplets of ethanol-water mixtures on gold surfaces modified with self-assembled monolayers., J. Phys. Chem. B. 110 (2006) 11267–71. doi:10.1021/jp0572885.

[22] L. Shi, P. Shen, D. Zhang, Q. Lin, Q. Jiang, Wetting and evaporation behaviors of water–ethanol sessile drops on PTFE surfaces, Surf. Interface Anal. 41 (2009) 951–955. doi:10.1002/SIA.3123.

[23] C. Liu, E. Bonaccurso, Microcantilever sensors for monitoring the evaporation of microdrops of pure liquids and mixtures, Rev. Sci. Instrum. 81 (2010) 13702. doi:10.1063/1.3276716.

[24] S.M. Rowan, M.I. Newton, F.W. Driewer, G. McHale, Evaporation of Microdroplets of Azeotropic Liquids, J. Phys. Chem. B. 104 (2000) 8217–8220. doi:10.1021/jp000938e.

[25] R. Vochten, G. Petre, Study of the heat of reversible adsorption at the air-solution interface. II. Experimental determination of the heat of reversible adsorption of some alcohols, J. Colloid Interface Sci. 42 (1973) 320–327. doi:10.1016/0021-9797(73)90295-6.

[26] A. Oron, P. Rosenau, On a nonlinear thermocapillary effect in thin liquid layers, J. Fluid Mech. 273 (1994) 361–374. doi:10.1017/S0022112094001977.

[27] S.G. Slavtchev, S.P. Miladinova, Thermocapillary flow in a liquid layer at minimum in surface tension, Acta Mech. 127 (1998) 209–224. doi:10.1007/BF01170374.

[28] Y. ABE, Self-Rewetting Fluids: Beneficial Aqueous Solutions, Ann. N. Y. Acad. Sci. 1077 (2006) 650–667. doi:10.1196/annals.1362.026.

[29] Y. Abe, A. Iwasaki, K. Tanaka, Microgravity experiments on phase change of self-rewetting fluids., Ann. N. Y. Acad. Sci. 1027 (2004) 269–85. doi:10.1196/annals.1324.022.

[30] N. di Francescantonio, R. Savino, Y. Abe, New alcohol solutions for heat pipes: Marangoni effect and heat transfer enhancement, Int. J. Heat Mass Transf. 51 (2008) 6199–6207. doi:10.1016/j.ijheatmasstransfer.2008.01.040.

[31] R. Di Paola, R. Savino, D. Mirabile Gattia, R. Marazzi, M. Vittori Antisari, Self-rewetting carbon nanofluid as working fluid for space and terrestrial heat pipes, J. Nanoparticle Res. 13 (2011) 6207–6216. doi:10.1007/s11051-011-0601-y.

[32] R. Savino, D. Paterna, Marangoni effect and heat pipe dry-out, Phys. Fluids. 18 (2006) 118103. doi:10.1063/1.2397586.

[33] R. Savino, A. Cecere, R. Di Paola, Surface tension-driven flow in wickless heat pipes with self-rewetting fluids, Int. J. Heat Fluid Flow. 30 (2009) 380–388. doi:10.1016/j.ijheatfluidflow.2009.01.009.

[34] R. Savino, N. di Francescantonio, R. Fortezza, Y. Abe, Heat pipes with binary mixtures and inverse Marangoni effects for microgravity applications, Acta Astronaut. 61 (2007) 16–26. doi:10.1016/j.actaastro.2007.01.002.

[35] K. Tanaka, Y. Abe, M. Nakagawa, C. Piccolo, R. Savino, Low-gravity experiments of lightweight flexible heat pipe panels with self-rewetting fluids., Ann. N. Y. Acad. Sci. 1161 (2009) 554–61. doi:10.1111/j.1749-6632.2008.04333.x.

[36] Y. Hu, T. Liu, X. Li, S. Wang, Heat transfer enhancement of micro oscillating heat pipes with self-rewetting fluid, Int. J. Heat Mass Transf. 70 (2014) 496–503. doi:10.1016/j.ijheatmasstransfer.2013.11.031.

[37] H. Ghasemi, C.A. Ward, Energy transport by thermocapillary convection during Sessile-Water-droplet evaporation., Phys. Rev. Lett. 105 (2010) 136102. doi:10.1103/PhysRevLett.105.136102.

[38] A. Sitar, I. Golobic, Heat transfer enhancement of self-rewetting aqueous n-butanol solutions boiling in microchannels, Int. J. Heat Mass Transf. 81 (2015) 198–206. doi:10.1016/j.ijheatmasstransfer.2014.10.034.

[39] M.E.R. Shanahan, K. Sefiane, Recalcitrant bubbles, Sci. Rep. 4 (2014). doi:10.1038/srep04727.

[40] T. Cubaud, C.M. Ho, Transport of bubbles in square microchannels, Phys. Fluids. 16 (2004) 4575–4585. doi:10.1063/1.1813871.

[41] T.N. Tran, M.W. Wambsganss, D.M. France, Small circular- and rectangular-channel boiling with two refrigerants, Int. J. Multiph. Flow. 22 (1996) 485–498. doi:10.1016/0301-9322(96)00002-X.

[42] S. Saisorn, S. Wongwises, The effects of channel diameter on flow pattern, void fraction and pressure drop of two-phase air–water flow in circular micro-channels, Exp. Therm. Fluid Sci. 34 (2010) 454–462. doi:10.1016/j.expthermflusci.2009.02.006.

[43] Y. Wang, K. Sefiane, Effects of heat flux, vapour quality, channel hydraulic diameter on flow boiling heat transfer in variable aspect ratio micro-channels using transparent heating, Int. J. Heat Mass Transf. 55 (2012) 2235–2243. doi:10.1016/j.ijheatmasstransfer.2012.01.044.

[44] A. Sur, D. Liu, Adiabatic air–water two-phase flow in circular microchannels, Int. J. Therm. Sci. 53 (2012) 18–34. doi:10.1016/j.ijthermalsci.2011.09.021.

[45] L. Malter, D.B. Langmuir, Resistance, Emissivities and Melting Point of Tantalum, Phys. Rev. 55 (1939) 743–747. doi:10.1103/PhysRev.55.743.

[46] R.D. Allen, L.F. Glasier, P.L. Jordan, Spectral Emissivity, Total Emissivity, and Thermal Conductivity of Molybdenum, Tantalum, and Tungsten above 2300°K, J. Appl. Phys. 31 (1960) 1382–1387. doi:10.1063/1.1735847.

[47] N.D. Milosevic, G.S. Vukovic, D.Z. Pavicic, K.D. Maglic, Thermal properties of tantalum between 300 and 2300 K, Int. J. Thermophys. 20 (1999) 1129–1136.

[48] R.P. Madding, Emissivity measurement and temperature correction accuracy considerations, in: D.H. LeMieux, J.R. Snell, Jr. (Eds.), International Society for Optics and Photonics, 1999: pp. 393–401. doi:10.1117/12.342307.

[49] J.C. Barber, Hydrodynamics, heat transfer and flow boiling instabilities in microchannels - Edinburgh University, The University of Edinburgh and Université d'Aix-Marseille I, 2009.

[50] Y. Wang, Liquid-vapour phase change and multiphase flow heat transfer in single micro-channels using pure liquids and nano-fluids, The University of Edinburgh, 2011.

[51] R.K. (Ramesh K.. Shah, A.L. (Alexander L. London, Laminar flow forced convection in ducts : a source book for compact heat exchanger analytical data, Academic Press, 1978.

[52] M. Thirumaleshwar, Fundamentals of heat and mass transfer, Dorling Kindersley, 2009.

[53] J.R. (John R. Taylor, An introduction to error analysis : the study of uncertainties in physical measurements, University Science Books, 1997.

[54] R. (Roland) Clift, J.R. Grace, M.E. Weber, Bubbles, drops, and particles, Academic Press, 1978.

[55] D. Bhaga, M.E. Weber, Bubbles in viscous liquids: shapes, wakes and velocities, J. Fluid Mech. 105 (1981) 61. doi:10.1017/S002211208100311X.

[56] F. Raymond, J.M. Rosant, A numerical and experimental study of the terminal velocity and shape of bubbles in viscous liquids, Chem. Eng. Sci. 55 (2000) 943–955. doi:10.1016/S0009-2509(99)00385-1.

[57] R. Balasubramaniam, A.T. Chai, Thermocapillary migration of droplets: An exact solution for small marangoni numbers, J. Colloid Interface Sci. 119 (1987) 531–538. doi:10.1016/0021-9797(87)90300-6.

[58] Z.B. Wu, W.R. Hu, Effects of Marangoni numbers on thermocapillary drop migration: Constant for quasi-steady state?, J. Math. Phys. 54 (2013) 23102. doi:10.1063/1.4792476.

[59] R. Balasubramaniam, R.S. Subramanian, The migration of a drop in a uniform temperature gradient at large Marangoni numbers, Phys. Fluids. 12 (2000) 733–743. doi:10.1063/1.870330.